Mathematical model for cartilage tissue-growth using a quadriphasic mixture and finite element analysis

by

Valentin Dhôte

B.S., École Spéciale de Travaux Publics, du Bâtiment et de l'Industrie

A thesis submitted to the

Faculty of the Graduate School of the

University of Colorado in partial fulfillment

of the requirements for the degree of

Master of Science

Department of Civil, Environmental, and Architectural Engineering

2012

This thesis entitled:
Mathematical model for cartilage tissue-growth using a quadriphasic mixture and finite element analysis
written by Valentin Dhôte
has been approved for the Department of Civil, Environmental, and Architectural Engineering

Franck J. Vernerey

Prof. Richard A. Regueiro

Prof. Stephanie J. Bryant

Date

The final copy of this thesis has been examined by the signatories, and we find that both the content and the form meet acceptable presentation standards of scholarly work in the above mentioned discipline.

Abstract

Dhôte, Valentin (M.S., Civil Engineering)

Mathematical model for cartilage tissue-growth using a quadriphasic mixture and finite element analysis

Thesis directed by Prof. Franck J. Vernerey

The goal of this thesis is to build a clear model of biological tissues growth, especially cartilage. But because tissues are complicated, simplifications and assumptions have to be made. In experiments, engineered tissues are often using hydrogels, because of their ability to mimic the real system. However, strategies to date are suboptimal in part because designing degradable hydrogels is complicated by structural and temporal complexities of the gel and evolving tissue along multiple length scales. To address this problem, this study proposes a multi-scale mechanical model using a quadriphasic formulation (solid, fluid, unbound matrix molecules, enzymes) based on a single chondrocyte releasing extracellular matrix molecules and enzymes within a degrading hydrogel. This model describes the key players of the biological system within the hydrogel encompassing different length scales. Different mechanisms are included: temporal changes of bulk properties due to hydrogel degradation, and matrix molecules transport. Numerical results show the competition between the diffusion of the matrix molecules and the the diffusion of the enzymes degrading the scaffold.

Acknowledgements

I would like first to thank Franck J. Vernerey, my advisor for his guidance on this project over the last eighteen months. I would like to thank Professors Regueiro and Bryant who accepted to be my committee members.

I would also aknowledge my research group Louis, Reza, Umut and Xavier for being helpful, helping me keep perspective and keeping a good atmosphere in our office. I would also like to thank everyone who was here during my past semesters for their serious and fun: Arnaud, Sophie, Scott, Yefgeniy, Xingang, Kevin, Florence and Antoine. I also thank Robin and my colleagues from my engineering school ESTP in France: Flavien, François, Olivier, Zaki, Pierre, Alexandre, Arnaud, Romain, Dalin and PA. Because we all took different paths.

I extend thanks to the University of Colorado at Boulder for providing courses of quality, all my professors and the administration of the CEAE department.

Lastly, I would like to thank my family without whose support none of this work would have been possible. To my mother Pascale, my father Robin, my sister Alix and my brother Basile. And especially to Alize for making my life wonderful. Thank you.

Contents

Tables

Figures

Chapter 1

Introduction

1.1 Why focusing on modeling

1.1.1 Complexity of the biological systems

With current surgical procedures offering imperfect solutions, new treatments are clearly warranted. Tissue engineering is one promising treatment option having for example the potential to yield living functional cartilage. Within this context, scaffolds are being developed to deliver cells (cartilage cells) to the damaged site and support new tissue deposition [37]. However, engineering functionally competent and well-integrated cartilage remains a hurdle, limiting clinical translation of cartilage tissue engineering.

Synthetic hydrogels hold much promise as a delivery vehicle for cells. However, tuning degradation to tissue growth has been challenging and as a result the engineered tissue is often mechanically inferior. This observation is further complicated by the fact that matrix synthesis rates and the size of matrix molecules can be highly variable depending on the cell type and age.

1.1.2 Modeling approach

A mathematical model can provide critical parameters for designing synthetic hydrogels to better match tissue growth for a particular cell source. Once the model is fully developed and validated, the model can be used to predict experimental results for a wide range of properties and degradation kinetics, thus dramatically reducing the number of experiments. Beyond this larger goal and the

specific model, a model can be helpful in other ways: simulations can predict what concentration of cells will yield a superior engineered tissue. The model can provide new insight into key mechanisms not obvious to experimentalists, such as osmotic pressure to enhance molecular diffusion. A model can, in combination with experimental results, predict values of kinetic parameters which are difficult to measure experimentally. The model can be a useful tool to optimize design parameters and to gain a better mechanical understanding.

1.2 Motivation and organization of this study

1.2.1 Theories involved

Theories of mixture and poro-elasticity have proven to be excellent frameworks onto which the deformation of tissues, such as cartilage, can be studied [1] [16] [23]. These theories have been investigated prior to developping the model [8] and allow to use a Lagrangian formulation where every phase are refering to the solid phase.

Continuum mechanics is naturally used to express the mechanics of the model and to express its behavior through equations, ie the governing equations.

To generalize the formulation, and because tissues can soak themselves to big strains or large swellings, the use of finite strain (large deformations) seems important.

1.2.2 Where do we stand

In cartilage, the problem of matrix diffusion, transport and deposition has been addressed at cellular [36] and tissue scales [11]. More recently, mathematical models have been expanded to cartilage tissue engineering strategies, predicting matrix diffusion from cells within scaffolds [40]. The problem of cell mediated gel degradation was also assessed with a triphasic mixture model [41] to better understand how degradation may affect both transport properties and gel mechanics. Finally, on a more global scale, a multiphasic model (made of linked ECM, scaffold and cells)

was used to derive a steady-state solution for tissue growth as a function of scaffold properties [14]. While the above studies have enabled a more quantitative understanding of the processes of synthesis, diffusion and deposition, few have considered the coupled physics of scaffold deformation, degradation and ECM transport for cells encapsulated in a degrading crosslinked hydrogel for which the size scale of porosity is of similar magnitude to that of many ECM molecules. Experimentally these processes have proven to be key in designing hydrogel scaffolds with encapsulated cells.

The main purpose of this thesis is to build a deep understanding of the growth in biological tissues, especially in cartilage. different approaches could be taken to reach this goal, but we want to build a strong model which is simple but reliable. The model should be simple enough so that it could be understood just by taking a look at its governing equation and a few figures. It can be a formulation other people could use.

The presentation of the work is organized as follows. First is explained how mixture theory combines the Lagrangian description and the referring to a phase. We then explain the physics of the scaffold used in the model: the hydrogel. Once all the bases are built, we develop the governing equations for our study. They are derived in chapter 2. Solid governing equation is first presented, followed by the other phases equations through on only equation. Chapter 3 discretizes the equations by the Finite Element Method, to get a system of coupled nonlinear equations governing the problem. Chapter 5 presents the numerical examples. Finally, results of the work and concluding remarks are summarized in chapter 6.

1.3 Modeling strategies

1.3.1 Mixture theory

The goal of poromechanics is to be able to understand the behavior of a system composed of both a solid and other materials. The typical system contains a solid phase, the skeleton, and a fluid saturing the porous space. The principle of superimposition is used to solve the problems. The

hypothesis of the mixture theory are that the physics behavior and the deformation are continuous.

Typically, a vector $\mathbf{X}$ defined in the reference or initial configuration is linked to itself in the current configuration $\mathbf{x}(\mathbf{X},t)$. This current vector can be mapped back to the initial configuration through the deformation gradient tensor $\mathbf{F}$: $d\mathbf{x} = \mathbf{F}d\mathbf{X}$.

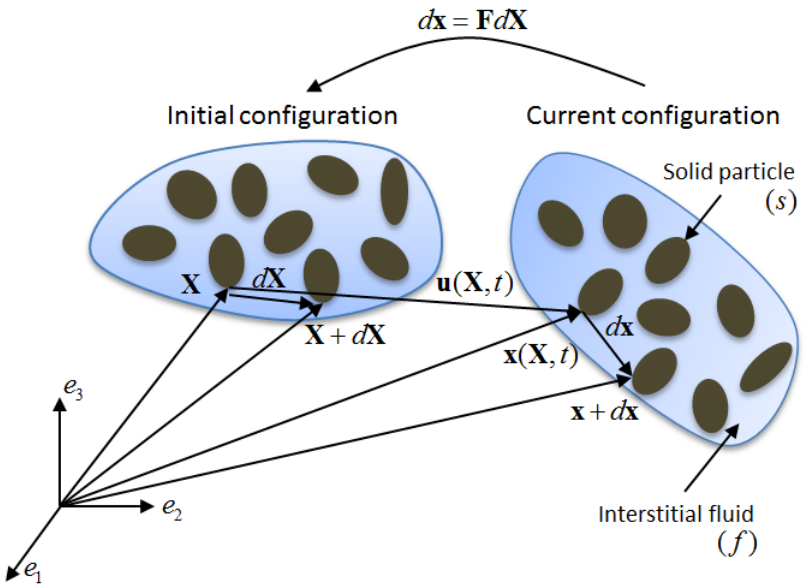

Figure 1.1: Coordinates in mixture theory

As mentionned earlier, the goal is to create a quadriphasic mixture, which means that each other phase will be taking the solid as a reference. Then, a relative velocity of the α phase is defined as

$$\tilde{\mathbf{v}}^{\alpha} = \mathbf{v}^{\alpha} - \mathbf{v}^{s} \tag{1.1}$$

1.3.2 Definition of our scaffold: the hydrogel

Hydrogels are crosslinked polymer networks with an average crosslink density ρ_x that influences the mechanical properties, degree of swelling, mesh size ξ, and subsequently transport properties. Polymers are long chains of repeating chemical units bonded together. When many polymer chains are amassed, they link together through crosslinks to form an elastic network whose characteristics

depend on the degree of polymerization (reaction between the mononomers to form the polymer chains), and the mesh size of the network. When plunged in a fluid, the latter occupies the space between the chains which soak until an equilibrium is reached. In other words, the polymer network swells when immerged in the fluid. A mixture is thus created and the polymer tends to dissolve. A particularity of the hydrogel (or polymer gel: the mixture of a polymer network with fluid) is that its polymers can absorb large quantity of water without dissolving [35].

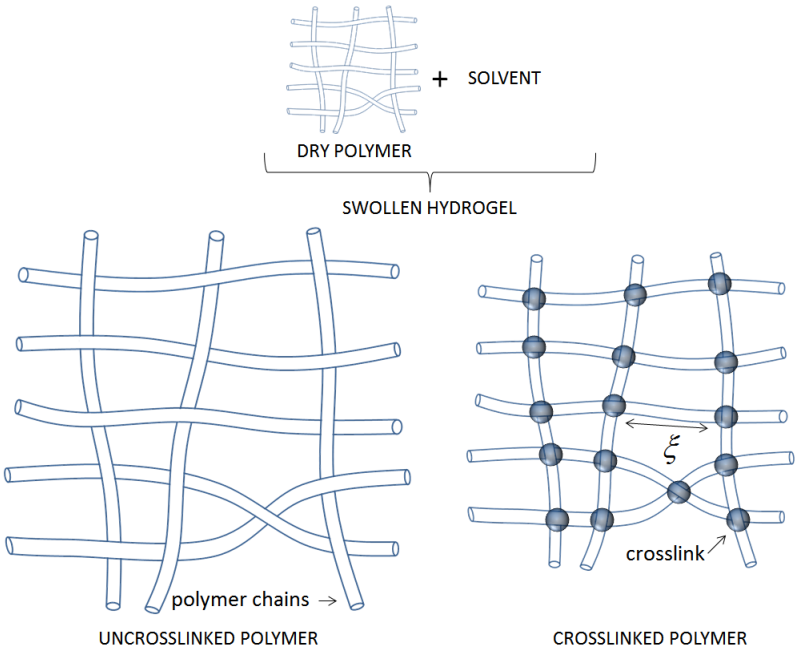

Figure 1.2: Network skeleton of the hydrogel

Because matrix molecules typically have high molecular weights, a large mesh size is often desirable to promote transport of these molecules through the gel for homogeneous tissue development. But, this leads to a mechanically inferior hydrogel. In contrast, a high crosslink density, which can conserve mechanical integrity is usually prohibitory to matrix molecules transport [32] [7].

Chapter 2

Thermodynamical formulation of the governing equations

Introduction

The goal of this chapter is to formulate the governing equations using a thermodynamical approach. A tissue can be easily described as crosslinked polymer chains, which is why it seems straight-forward to follow Flory theory [13] and use its thermodynamic lattice model based on statistical mechanics. A thermodynamical model and mixture theory allow to combine mechanical (continuum theories) and chemical forces (chemistry principles from thermodynamic) a tissue undergoes.

2.1 Thermodynamical model

It is assumed that a tissue can be modeled by a multiphasic mixture. The main phases are the scaffold, ie the polymer, and the fluid phase. But other phases can be added to describe particular reactions, such as transport or diffusion.

2.1.1 Gibbs free energy

To describe the mixture it is common in continuum mechanics to use a free energy function as described by the Flory-Rehner and rubber elasticity theories [13][39]. In the case of biological tissue, following Flory's theory on polymer networks [13], the Gibbs free energy ΔG will be used. Based on theories of swelling [9] the free energy of a swollen gel can be decomposed in two different contributions (see Fig. 2.1).

2.1.1.1 Elastic free energy

First, the elastic free energy $\Delta G^{el}(\mathbf{F})$ or the elasticity of the network, a configurational contribution (resisting pressure if the network swells). It is a function of the deformation gradient $\mathbf{F}(\mathbf{X}, t)$ only. Secondly, the free energy of mixing $\Delta G^{mix}(C^s, C^f, C^m, C^e)$ coming from the mixing of the different constituents - polymer (s), solvent (f), ECM molecules (m), enzymes (e) - is a function of the nominal concentrations $C^\alpha(t), \alpha = s, f, m, e$.

$$\Delta G(\mathbf{F}, C^s, C^f, C^m, C^e) = \Delta G^{el}(\mathbf{F}) + \Delta G^{mix}(C^s, C^f, C^m, C^e) \tag{2.1}$$

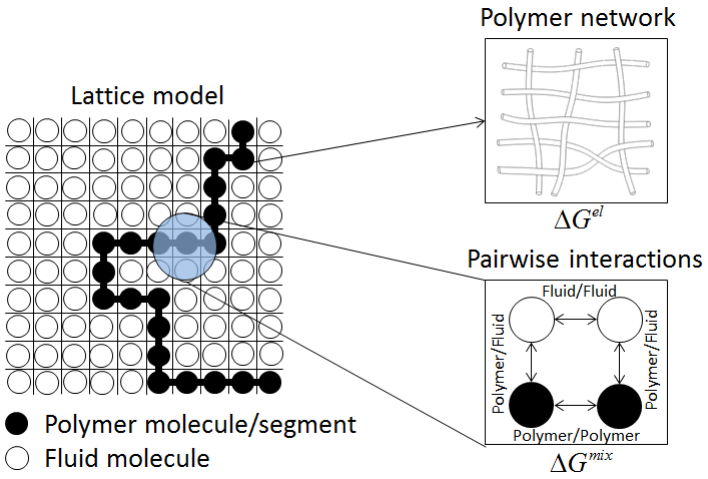

Figure 2.1: Different contributions of the Gibbs free energy.

The elastic contribution is defined by Flory [13] and Treloar [39], neglecting the phantom network theory [5] for simplicity:

$$\Delta G^{el}(\mathbf{F}) = \frac{1}{2} G \left(\lambda_1^2 + \lambda_2^2 + \lambda_3^2 - 3 - 2\ln\left(\lambda_1\lambda_2\lambda_3\right)\right) \quad \text{where} \quad G = \rho\overline{\nu}\rho_X RT \tag{2.2}$$

where $\lambda_1, \lambda_2, \lambda_3$ are the principal streches of the right deformation gradient tensor $\mathbf{F}(\mathbf{X}, t)$ in the principal directions. We note that $\lambda_1\lambda_2\lambda_3 = 1$ when the transformation is isochoric and then ΔG^{el} becomes the free energy of a Neo-Hookean material. However, when the polymer and the

water are mixed, the product $\lambda_1\lambda_2\lambda_3$ can become large and have a strong effect on the mechanical response of the mixture. A factor 2 is placed in front of the term $\ln(\lambda_1\lambda_2\lambda_3)$ in order to assure a stress equal to zero for an isochoric deformation. The shear modulus G can be expressed as a function of the specific volume of the solvent $\overline{\nu}$ (inverse of density), the crosslink density ρ_X of the swollen network, the polymer density ρ (dry polymer), the gas constant R and the temperature T.

2.1.1.2 Free energy of mixing

In order to model the enzymatic degradation of the scaffold and to mimic the matrix molecules deposition which are responsible for the creation of the PCM first and then the ECM, the Gibbs free energy of mixing is derived using the Flory-Huggins lattice model [13]. The model is assumed as a mixture of four phases but can be extended if more phases are required. An extended mixing contribution to the Gibbs free energy [6] can be written for the quaternary model:

$$\Delta G^{mix}(C^s, C^f, C^m, C^e) = H_0^{mix} + \Delta H^{mix} - T\Delta S^{mix} \tag{2.3}$$

where H_0 denotes the reference enthalpy of the quaternary model

$$\frac{H_0^{mix}}{V_0} = \sum_\alpha C^\alpha \mu_\alpha^0 \tag{2.4}$$

The entropy of mixing is calculated statistically by looking at the organization of the different species in the lattice model

$$\frac{\Delta S^{mix}}{V_0} = -k_B \sum_\alpha C^\alpha \ln \phi^\alpha \quad ; \quad C^\alpha = \frac{N^\alpha}{V_0} \tag{2.5}$$

where C^α is the concentration of the α phase with reference to the initial configuration, k_B is the Bolztmann constant, ϕ^α is the volume fraction, and V_0 is the total volume in the reference configuration. In addition, because the polymer solution cannot be considered as an ideal solution,

and that the entropy of mixing does not take into account the interactions solvent/polymer, which are not negligible, the enthalpy of mixing needs to be included. Yet, the other interactions between the different phases are assumed negligeable compared to the ones between the polymer chains and the solvent. The lattice model considering the interactions between nearest neighbors only, Flory-Huggins theory [13] expresses the enthalpy of mixing by the change in interaction energy resulting from the mixing.

$$\Delta H^{mix} = (z-2)N^f \phi^s \Delta w_{sf} \tag{2.6}$$

where z is the number of direct neighbors of a polymer molecule in the lattice model (e.g. for a square lattice model $z = 4$ and for a cubic lattice model $z = 6$). Then $(z-2)$ denotes the number of neighbors of a polymer segment, neglecting chain ends. Δw_{sf} is the change in interaction energy between a polymer chain and the solvent after mixing. This expression is usually written as

$$\Delta H^{mix} = k_B T \left(\chi_{sf} N^f \phi^s\right) \quad ; \quad \chi_{sf} = \frac{(z-2)\Delta w_{sf}}{k_B T} \tag{2.7}$$

where χ_{sf} is the binary (polymer-fluid interaction) Flory-Huggins parameter, i.e. it depends only on ϕ^s and ϕ^f. Note a positive value means that polymer-polymer and solvent-solvent contacts are prefered.

Thus, we get the final form of the volumetric Gibbs free energy of mixing ($\Delta G^{mix}/V_0$), which is from what we will refer to as the total Gibbs free energy of mixing:

$$\Delta G^{mix}(C^\alpha) = \sum_\alpha C^\alpha \mu_\alpha^0 + k_B T \sum_\alpha C^\alpha \ln \phi^\alpha + k_B T \chi_{sf} C^f \phi^s \tag{2.8}$$

2.1.2 Molecular incompressibility

It is assumed that the swelling ratio J of the mixture equals 1 when the polymer is dry and no other phases are involved. When other phases are added, their contributions to the swelling ratio are taking into account through the molecular incompressibility assumption [17]:

$$J = 1 + \sum_{\alpha} \nu^{\alpha} C^{\alpha} \tag{2.9}$$

where the reference concentration C^{α} are defined as

$$C^{\alpha} = \frac{N^{\alpha}}{V_0} = \eta^{\alpha}\phi^{\alpha} \quad , \quad \eta^{\alpha} = \frac{N^{\alpha}}{V^{\alpha}} \tag{2.10}$$

2.1.3 Modified Gibbs free energy

For ease of implementation, the molecular incompressibility (Eq. (2.9)) is used to solve the problem. It is enforced by adding a term to the Gibbs free energy of the system using a Lagrange multiplyer π:

$$\Delta\hat{G}(\mathbf{F}, C^{\alpha}) = \Delta G(\mathbf{F}, C^{\alpha}) - \pi \left(J - 1 - \sum_{\alpha} \nu^{\alpha} C^{\alpha} \right) \tag{2.11}$$

Then, we can use the free energy function to define the first Piola-Kirchhoff stress tensor:

$$\mathbf{P} = \frac{\partial \Delta\hat{G}(\mathbf{F}, C^{\alpha})}{\partial \mathbf{F}} = \frac{\partial \Delta G^{el}(\mathbf{F})}{\partial \mathbf{F}} - J\mathbf{F}^{-T}\pi \tag{2.12}$$

2.1.4 Chemical potential

By taking the derivative of Eq. (2.11) with respect to C^{α} one can show that the chemical potential for the α phase depends on the osmotic pressure, i.e. the Lagrange multiplyer:

$$\mu_{\alpha} = \left(\frac{\Delta\hat{G}(\mathbf{F}, C^{\alpha})}{\partial C^{\alpha}} \right)_{C^{\beta}, \beta \neq \alpha} \tag{2.13}$$

$$\mu_{\alpha} = \mu_{\alpha}^{0} + k_B T \ln \phi^{\alpha} + \pi\nu^{\alpha} \quad , \quad \alpha \neq f \tag{2.14}$$

$$\mu_{f} = \mu_{f}^{0} + k_B T \ln \phi^{f} + k_B T \chi_{sf} \phi^{s} + \pi\nu^{\alpha} \tag{2.15}$$

2.1.5 Osmotic pressure

The osmotic pressure is defined to be consistent with the definitions of stress. It is well known that the Cauchy stress σ is related to the 2nd Piola-Kirchhoff stress $\mathbf{S}$ by the relation:

$$\mathbf{S} = J\mathbf{F}^{-1}\sigma\mathbf{F}^{-T} \tag{2.16}$$

Then, we define a "Cauchy osmotic pressure" π and a "Piola-Kirchhoff osmotic pressure" Π by

$$\mathbf{\Pi} = J\mathbf{F}^{-1}\pi\mathbf{F}^{-T} \tag{2.17}$$

This relation will be used in Chapter 3 to linearize the weak form.

2.1.6 Balance of linear momentum

The balance of linear momentum gives the mechanical strong form:

$$\boldsymbol{\nabla}_{\mathbf{X}} \cdot \mathbf{P} + \mathbf{b}_0 = 0 \tag{2.18}$$

where $\boldsymbol{\nabla}_{\mathbf{X}}\cdot$ refers to the divergence operator, with respect to the reference (initial) configuration, ie the dry state, where $\mathbf{X}$ is the material vector and $\mathbf{b}_0$ is the body force. The first Piola-Kirchhoff stress is denoted by $\mathbf{P}$.

2.1.7 Balance of mass

The balance of mass of the molecules shows that their number is conserved. Namely:

$$\frac{D^s C^\alpha(\mathbf{X},t)}{Dt} + \boldsymbol{\nabla}_{\mathbf{X}} \cdot \mathbf{Q}^\alpha(\mathbf{X},t) = 0 \tag{2.19}$$

where D^s denotes the material derivative with respect to the solid (polymer) phase. From a modeling point of view, transport of the fluid (f) and of unbound extracellular matrix molecules (p) can be described by their volumetric flux, taken with respect to polymer motion:

$$\mathbf{q}^\alpha = \phi^\alpha \tilde{\mathbf{v}}^\alpha = \phi^\alpha (\mathbf{v}^\alpha - \mathbf{v}^s) \tag{2.20}$$

Note that the flux is defined as the volume of constituent α per unit of time, passing through a unit surface S in the deformed configuration. When large deformations are considered, however, it is convenient to define the Lagrangian flux

$$\mathbf{Q}^\alpha = J\mathbf{F}^{-1}\mathbf{q}^\alpha \tag{2.21}$$

as the amount of constituent passing through a unit area in the reference gel configuration (defined in the dry state, i.e. initial configuration). Eq. 2.21 therefore shows the mapping of the flux from the current configuration to the dry polymer configuration.

2.1.8 Transport and diffusion

2.1.8.1 Flux of molecules of the α phase

According to thermodynamics, diffusion is assumed to occur in order to minimize the free energy ΔG. Following the definition of the chemical potential in Eq. (2.13), the free energy gradient can be expressed through the chemical potential gradient. Thus the flux of molecules is driven by removing the differences in chemical potential:

$$\mathbf{Q}^\alpha = -\mathbf{D}^\alpha C^\alpha \boldsymbol{\nabla}_{\mathbf{X}} \mu_\alpha(\mathbf{X}, t) \tag{2.22}$$

where $\mathbf{D}^\alpha$ is the fluid diffusion tensor, or mobility tensor (atomic mobility of the molecules), and μ_α is the chemical potential. It gives the expression of the diffusion flux of molecules alpha $\mathbf{Q}^\alpha$ by reinjecting Eq. (2.15) in Eq. (2.22):

$$\mathbf{Q}^{\alpha} = -\mathbf{D}^{\alpha}\left(k_B T \boldsymbol{\nabla}_{\mathbf{X}} C^{\alpha} + \nu^{\alpha} C^{\alpha} \boldsymbol{\nabla}_{\mathbf{X}} \pi\right) \tag{2.23}$$

It shows that the flux of the α phase is expressed as the summation of Fick's law (first term driven by the gradient of the concentration) and Darcy's law (second term driven by the gradient of the pressure).

2.1.8.2 Diffusion of the molecules of fluid

An important aspect of the present study is the introduction of realistic constitutive relations governing the transport of ECM molecules and water through the gel and their relation to gel deformation and degradation. The diffusivity of the fluid is attributed to the permeability of the gel:

$$D^f = \frac{\xi^2(1-\phi^s)}{8\bar{\mu}_f \delta} \tag{2.24}$$

where δ is the tortuosity of the gel structure and $\bar{\mu}_f$ is the fluid viscosity. We note that the gel permeability to water is a function of polymer mesh size [16], which is itself a function of gel crosslinking and can be related to swelling. This dependency was introduced by Bell and Peppas [5] as follows:

$$\xi = \xi_0 (\phi^s)^{-1/4} \quad ; \quad \xi_0 = {C_n}^{1/2} n^{1/2} l \tag{2.25}$$

where ξ is the mesh size of the dry polymer, l is the average bond length, C_n is the polymer characteristic ratio, and n is the number of bonds between crosslinks, which is determined from the molecular weight between crosslinks and molecular weight of the polymer repeat unit. It is clear from Eq. (2.24) and (2.25) that gel swelling (through hydrolytic degradation for instance), by decreasing the value of ϕ^s, ultimately increases gel permeability and facilitates transport of water through the hydrogel. But also, the number of bonds between crosslinks changes with changes in crosslink density [13], which means that the mesh size evolves with degradation.

2.1.8.3 Diffusion of the matrix molecules and enzymes

Lustig and Peppas [27] have developped a reliable model to describe the diffusibility of a solute in a crosslinked hydrogel. The diffusivity coefficient proposed is

$$D^{\alpha} = D_{\infty}\left(1 - \frac{r_s}{\xi}\right) exp\left(-Y\frac{\phi^s}{1-\phi^s}\right) \tag{2.26}$$

where r_s is the radius of gyration of small matrix molecules, ξ is the mesh size, ϕ^s is the volume fraction of the solid and Y is a correction factor. The Stokes-Einstein equations gives the free solution diffusivity D_{∞}:

$$D_{\infty} = \frac{k_B T}{6\pi\bar{\mu_f} r_s} \tag{2.27}$$

where k_B is the Boltzmann constant, T is the temperature and $\bar{\mu_f}$ is the fluid viscosity. The effect of the gel resistance on molecule transport can then be captured by realizing that when the ratio of radius of gyration r_s of molecules is significantly smaller than the polymer mesh size ($r_s/\xi << 1$), gel resistance is negligible and the molecule flux $\mathbf{q}^{\alpha}$, $\alpha \neq f$ becomes $\mathbf{q}^{\alpha}_{\infty}$. However, as r_s increases, we assume that gel resistance results in a decrease of the flux that is expressed in the form:

$$\mathbf{q}^{\alpha} = g(\xi)\mathbf{q}^{\alpha}_{\infty} \tag{2.28}$$

The function g used in this study attempts to capture the nonlinear relationship between ECM transport processes and the relative sizes of ECM molecules and hydrogel mesh. As shown in Fig. 2.2, this function clearly implies that (1) as molecules become larger than the hydrogel mesh size, molecules transport is fully hindered ($g \longrightarrow 0$) and (2) as the hydrogel mesh size becomes significantly larger than the molecules size, gel resistance becomes negligible ($g \longrightarrow 1$). This expression was originally motivated by the work of Lustig and Peppas in [27] in their method to describe the change in diffusivity with the ratio r_s/ξ.

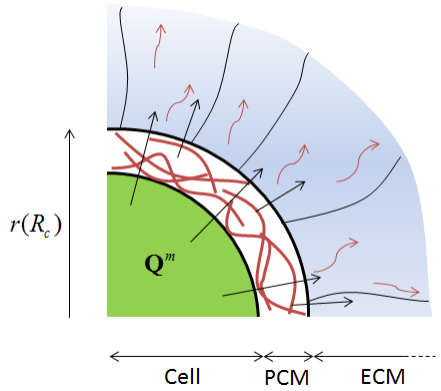

Figure 2.2: Diffusivity of proteins through the hydrogel. How the size of a protein impacts the boundary conditions.

2.1.9 Degradation of the scaffold

2.1.9.1 Hydrolytic degradation

During degradation, the macroscopic properties of the hydrogel evolve dynamically. As a first approach, hydrolytic degradation is described by pseudo first-order kinetics [29], where crosslink density decreases with degradation time:

$$\frac{D^s \rho_X}{Dt} = -k\rho_X \tag{2.29}$$

where k is the pseudo first order rate constant for hydrolytic degradation. Thus as time evolves, crosslinks degrade randomly within the gel, which leads to decreases in the shear elastic modulus G (Eq. (2.2)) but increases in swelling and mesh size, where the latter improves transport of ECM molecules through the gel. It is important to note that this model represents a simplified model for degradation kinetics. As such, it does not capture more subtle elements of degradation such as the phenomenon of reverse gelation. Reverse gelation refers to the point when there are fewer than two crosslinks per kinetic chain resulting in highly branched soluble polymer chains [13]. While not explicitly incorporated into this equation, the importance of this physical point should not be underestimated as it has the potential to dramatically influence how well macroscopic tissue

can form prior to reverse gelation.

2.1.9.2 Enzymatic degradation

But in reality, the inner cell secretes enzymes in time to enable the diffusion of its matrix molecules. This degradation in hydrogels has been shown to describe a Michaelis-Menten degradation [25]:

$$\frac{D^s \rho_X}{Dt} = -\frac{k_2 C^e \rho_X}{K_m + \rho_X} \tag{2.30}$$

where k_2 and K_m are the Michaelis degradation constants. The degradation of the polymer, which depends on the concentration of enzymes, is spatially dependant. The enzymes have the ability of breaking crosslinks, decreasing the crosslink density as they diffuse through the gel.

As a result for the combination of both hydrolytic and enzymatic degradation, the degradation follows the equation below:

$$\frac{D^s \rho_X}{Dt} = -k\rho_X - \frac{k_2 C^e \rho_X}{K_m + \rho_X} \tag{2.31}$$

2.2 Summary of the governing equations

Balance of linear momentum

$$\boldsymbol{\nabla}_{\mathbf{X}} \cdot \mathbf{P} + \mathbf{b}_0 = 0 \tag{2.32}$$

Balance of mass

$$\frac{DC^{\alpha}(\mathbf{X},t)}{Dt} + \boldsymbol{\nabla}_{\mathbf{X}} \cdot \mathbf{Q}^{\alpha}(\mathbf{X},t) = 0 \tag{2.33}$$

Molecular incompressibility

$$J = 1 + \sum_{\alpha} \nu^{\alpha} C^{\alpha} \tag{2.34}$$

Total Gibbs free energy

$$\Delta\hat{G}(\mathbf{F}, C^{\alpha}) = \Delta G^{el}(\mathbf{F}) + \Delta G^{mix}(C^{\alpha}) - \pi \left(J - 1 - \sum_{\alpha} \nu^{\alpha} C^{\alpha} \right) \tag{2.35}$$

$$\Delta G^{el}(\mathbf{F}) = \frac{1}{2} G \left(\lambda_1^2 + \lambda_2^2 + \lambda_3^2 - 3 - 2\ln\left(\lambda_1\lambda_2\lambda_3\right) \right) \quad \text{where} \quad G = \rho\overline{\nu}\rho_X RT \tag{2.36}$$

$$\Delta G^{mix}(C^{\alpha}) = \sum_{\alpha} C^{\alpha}\mu_{\alpha}^{0} + k_B T \sum_{\alpha} C^{\alpha} \ln\phi^{\alpha} + k_B T \chi_{sf} C^{f} \phi^{s} \tag{2.37}$$

Chapter 3

Finite Element discretization and numerical solution

Introduction

The problem defined by the governing equations can not be solved analytically. A numerical solution procedure is needed. Section 3.1 discretizes the governing equations in space and in time to obtain a set of discrete equations representing the problem.

3.1 Setting up the problem

In this study, the first important step is to create a numerically solvable model. Because of the complexity of the biological system, assumptions have to be made. But these assumptions still have to capture the key players.

3.1.1 From the biological system to the model

Multiscale computational modeling was employed to understand key microscopic processes driving tissue growth in terms of hydrogel structure, degradation and cell density. At the tissue level, these processes may be entirely described by continuous field equations in terms of hydrogel displacement u, solvent pressure π, concentration c^α of molecules ($\alpha = f, m, e$ fluid, matrix molecules, enzymes), all functions of location $\mathbf{X}$ and time t. To reduce the complexity of the problem, a homogeneous cell distribution was considered such that the analysis of the entire tissue could be summarized by a model volume consisting of a single spherical chondrocyte of radius R_c embedded

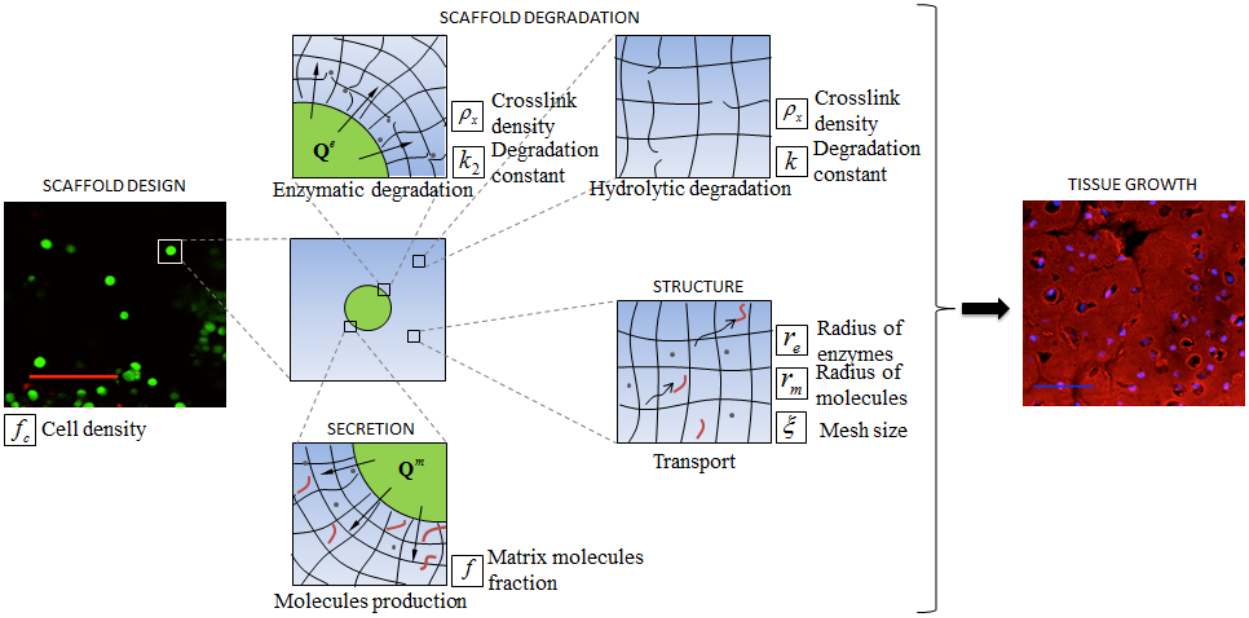

Figure 3.1: Mutiscale approach to modeling tissue production by cells encapsulated in hydrogels. Refer to the next sections for the parameters.

in a spherical hydrogel domain with radius R_g. Overall cell volume fraction, f_c, (Fig. 3.2) can then be described through the relation:

$$R_c/R_g = (f_c)^{1/3} \tag{3.1}$$

In spherical coordinates, the fields are functions of R, θ and ϕ. However, in this simplified system, under centro-symmetric assumption, the continuous fields only depend on the distance R from the center of the chondrocyte (in the initial, dry state). The macroscopic problem therefore consists of evaluating the evolution of the following three fields:

$$u(R,t), \pi(R,t), c^{\alpha}(R,t) \qquad \alpha = f, m, e \tag{3.2}$$

These fields evolve as a result of the constant release of ECM molecules en enzymes by chondrocytes from the cell membrane and changes in the osmotic swelling of the hydrogel resulting from bulk and enzymatic degradation. As explained later, the combination of degradation and

ECM production that results in the growth and organization of the new tissue is highly dependent on the initial hydrogel structure and the design of its degradation through the number of degradable linkages.

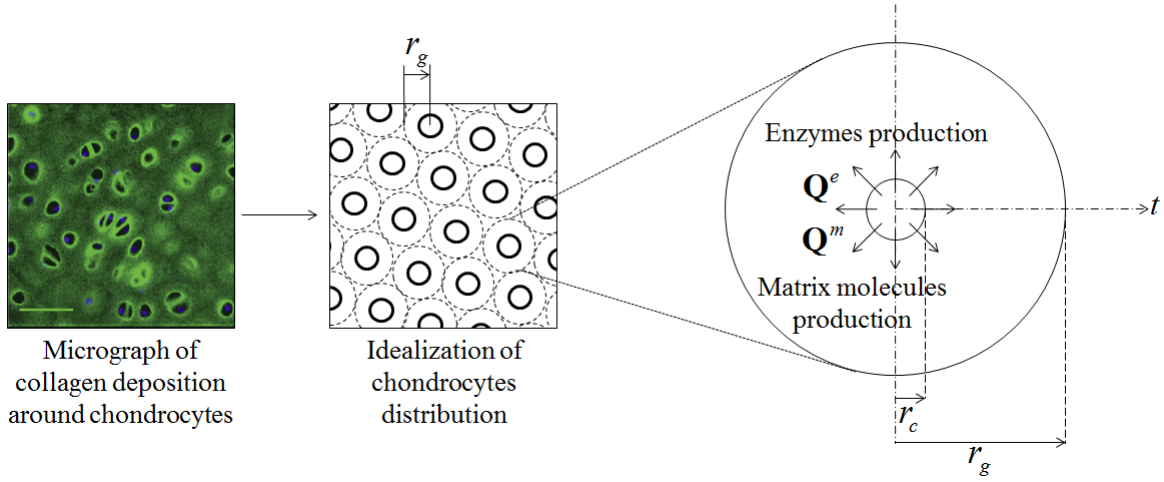

Figure 3.2: From real engineered tissues to an idealized mathematical model. Left picture shows cell nuclei (blue) and collagen (green). Scale bar represents $50\mu m$.

3.1.2 A multiphasic model

The crosslinked polymer network of the hydrogel can be considered as a hydrated elastic solid whose mechanics highly depend on the underlying molecular structure [5]. To represent hydrogel degradation and tissue growth, the hydrogel was considered as a mixture [41] of different phases that consists of the solid (or polymer) phase, the fluid (or solvent) phase, the unbound matrix molecules (proteoglycans, collagens) phase, and the enzymes phase. Consistent with mixture theory, each phase (denoted by $\alpha = s, f, m, e$, respectively) is described with its volume fraction ϕ^α such that

$$\sum_\alpha \phi^\alpha = 1 \quad \text{and} \quad \phi^\alpha << 1, \alpha = m, e \tag{3.3}$$

This equation implies that each phase is saturated within the mixture. It is also reasonable to assume that each phase is incompresssible at the microscopic level due to the relatively low physiological pressure encountered *in vivo*. In other words, the true mass density $\rho^{\alpha R}$ of various

phases remains constant during the growth process. Growth can however be measured by the change in effective mass density representing the mass of each phase per unit volume of mixture through the relation:

$$\rho^{\alpha}(R) = \phi^{\alpha}(R)\rho^{\alpha R}(R) \tag{3.4}$$

3.2 Weak form

3.2.1 Solid phase

For the solid phase, it is common to start from Eq. (2.32); the strong form is multiplyed by the weighting function $\delta\mathbf{z}$ and integrated over the reference spatial domain (initial configuraiton) Ω_0:

$$\int_{\Omega_0} \boldsymbol{\nabla}_{\mathbf{X}} \cdot \mathbf{P}\delta\mathbf{z} + \int_{\Omega_0} \mathbf{b}_0\delta\mathbf{z} = 0 \tag{3.5}$$

The divergence theorem is applied and leads to

$$\int_{\Omega_0} \mathbf{P} : (\boldsymbol{\nabla}_{\mathbf{X}}\delta\mathbf{z})dV_0 = \int_{\Omega_0} \mathbf{b}_0 \cdot \delta\mathbf{z}dV_0 + \int_{\Gamma_0} \mathbf{t}_0 \cdot \delta\mathbf{z}dS_0 \tag{3.6}$$

3.2.2 Alpha phase

Starting from Eq. (2.33), multiplying it by a weighing function δw and integrating over the spacial domain Ω_0:

$$\begin{aligned}\int_{\Omega_0} \frac{\partial C^{\alpha}}{\partial t}\delta w dV_0 + \int_{\Omega_0} \mathbf{v} \cdot \boldsymbol{\nabla}_{\mathbf{X}} C^{\alpha}\delta w dV_0 \\ - \int_{\Omega_0} \boldsymbol{\nabla}_{\mathbf{X}} \cdot \mathbf{D}^{\alpha} k_B T \boldsymbol{\nabla}_{\mathbf{X}} C^{\alpha}\delta w dV_0 - \int_{\Omega_0} \boldsymbol{\nabla}_{\mathbf{X}} \cdot \mathbf{D}^{\alpha}\nu^{\alpha}C^{\alpha}\boldsymbol{\nabla}_{\mathbf{X}}\pi\delta w dV_0 = 0\end{aligned} \tag{3.7}$$

Applying the divergence theorem on the 2nd and 3rd terms:

$$\int_{\Omega_0} \frac{\partial C^\alpha}{\partial t}\delta w dV_0 + \int_{\Omega_0} \dot{\mathbf{u}} \cdot \boldsymbol{\nabla}_{\mathbf{X}} C^\alpha \delta w dV_0 + \int_{\Omega_0} (\mathbf{D}^\alpha k_B T \boldsymbol{\nabla}_{\mathbf{X}} C^\alpha) \cdot \boldsymbol{\nabla}_{\mathbf{X}} \delta w dV_0 + \int_{\Omega_0} (\mathbf{D}^\alpha \nu^\alpha C^\alpha \boldsymbol{\nabla}_{\mathbf{X}} \pi) \cdot \boldsymbol{\nabla}_{\mathbf{X}} \delta w dV_0 = \int_{\Omega_0} \boldsymbol{\nabla}_{\mathbf{X}} \cdot (\mathbf{D}^\alpha k_B T \boldsymbol{\nabla}_{\mathbf{X}} C^\alpha \delta w)\, dV_0 + \int_{\Omega_0} \boldsymbol{\nabla}_{\mathbf{X}} \cdot (\mathbf{D}^\alpha \nu^\alpha C^\alpha \boldsymbol{\nabla}_{\mathbf{X}} \pi \delta w)\, dV_0 \quad (3.8)$$

which gives

$$\int_{\Omega_0} \frac{\partial C^\alpha}{\partial t}\delta w dV_0 + \int_{\Omega_0} \dot{\mathbf{u}} \cdot \boldsymbol{\nabla}_{\mathbf{X}} C^\alpha \delta w dV_0 + \int_{\Omega_0} (\mathbf{D}^\alpha k_B T \boldsymbol{\nabla}_{\mathbf{X}} C^\alpha) \cdot \boldsymbol{\nabla}_{\mathbf{X}} \delta w dV_0 + \int_{\Omega_0} (\mathbf{D}^\alpha \nu^\alpha C^\alpha \boldsymbol{\nabla}_{\mathbf{X}} \pi) \cdot \boldsymbol{\nabla}_{\mathbf{X}} \delta w dV_0 = \int_{\Gamma_0} \mathbf{D}^\alpha k_B T \boldsymbol{\nabla}_{\mathbf{X}} C^\alpha \delta w \cdot \mathbf{n}_0 dS_0 + \int_{\Gamma_0} \mathbf{D}^\alpha \nu^\alpha C^\alpha \boldsymbol{\nabla}_{\mathbf{X}} \pi \delta w \cdot \mathbf{n}_0 dS_0 \quad (3.9)$$

A flux of solvent molecules, $i^\alpha(\mathbf{X}, t)$ is going through the surface of the gel, where $\mathbf{n}_0$ is the unit normal vector in the reference configuration. This flux can be defined as:

$$i_0(\mathbf{X}, t) = (\mathbf{D}^\alpha k_B T \boldsymbol{\nabla}_{\mathbf{X}} C^\alpha + \mathbf{D}^\alpha \nu^\alpha C^\alpha \boldsymbol{\nabla}_{\mathbf{X}} \pi) \cdot \mathbf{n}_0(\mathbf{X}) \quad (3.10)$$

The weak form of the fluid takes the form:

$$\int_{\Omega_0} \frac{\partial C^\alpha}{\partial t}\delta w dV_0 + \int_{\Omega_0} \dot{\mathbf{u}} \cdot \boldsymbol{\nabla}_{\mathbf{X}} C^\alpha \delta w dV_0 + \int_{\Omega_0} (\mathbf{D}^\alpha k_B T \boldsymbol{\nabla}_{\mathbf{X}} C^\alpha) \cdot \boldsymbol{\nabla}_{\mathbf{X}} \delta w dV_0 + \int_{\Omega_0} (\mathbf{D}^\alpha \nu^\alpha C^\alpha \boldsymbol{\nabla}_{\mathbf{X}} \pi) \cdot \boldsymbol{\nabla}_{\mathbf{X}} \delta w dV_0 = -\int_{\Gamma_0} i_0 \delta w dS_0 \quad (3.11)$$

3.2.3 Molecular incompressibility

The molecular incompressibility equation, Eq. (2.34), is multiplyed by a weighting function $\delta\xi$ and integrated over the inirial spatial domain Ω_0:

$$\int_{\Omega_0} \left(J - 1 - \sum_\alpha \nu^\alpha C^\alpha \right) \delta\xi dV_0 = 0 \tag{3.12}$$

3.2.4 Summary of the Weak form

Solid

$$\int_{\Omega_0} \mathbf{P} : (\boldsymbol{\nabla}_\mathbf{X} \delta\mathbf{z}) dV_0 = \int_{\Omega_0} \mathbf{b}_0 \cdot \delta\mathbf{z} dV_0 + \int_{\Gamma_0} \mathbf{t}_0 \cdot \delta\mathbf{z} dS_0 \tag{3.13}$$

Alpha phase

$$\begin{aligned} \int_{\Omega_0} \frac{\partial C^\alpha}{\partial t} \delta w dV_0 + \int_{\Omega_0} \dot{\mathbf{u}} \cdot \boldsymbol{\nabla}_\mathbf{X} C^\alpha \delta w dV_0 \\ + \int_{\Omega_0} (\mathbf{D}^\alpha k_B T \boldsymbol{\nabla}_\mathbf{X} C^\alpha) \cdot \boldsymbol{\nabla}_\mathbf{X} \delta w dV_0 + \int_{\Omega_0} (\mathbf{D}^\alpha \nu^\alpha C^\alpha \boldsymbol{\nabla}_\mathbf{X} \pi) \cdot \boldsymbol{\nabla}_\mathbf{X} \delta w dV_0 \\ = - \int_{\Gamma_0} i_0 \delta w dS_0 \end{aligned} \tag{3.14}$$

Molecular incompressibility

$$\int_{\Omega_0} \left(J - 1 - \sum_\alpha \nu^\alpha C^\alpha \right) \delta\xi dV_0 = 0 \tag{3.15}$$

3.3 Galerkin form

3.3.1 Unknowns discretization

A mixed formulation is used with three-node elements for the solid phase, and two-node elements for the other unknowns. Then, shape functions N and N_0 and their derivatives B, B_1 and B_0 are defined in spherical coordinates because under isotropic assumptions only r and θ directions are investigated. No need to look at the ψ direction as it is the same as the θ one. For example, the first Piola-Kirchhoff stress $\mathbf{P}$ will be refered as by the vector $[P_{RR} \quad P_{\theta\theta}]^T$.

The mixed formulation can be summarized for each phase by showing the nodal values of each phase in an element:

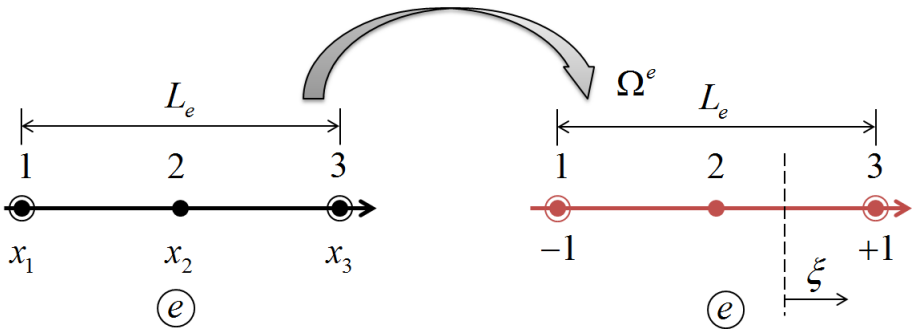

Figure 3.3: Representation of the mapping of an element between the physical and parent coordinate system.

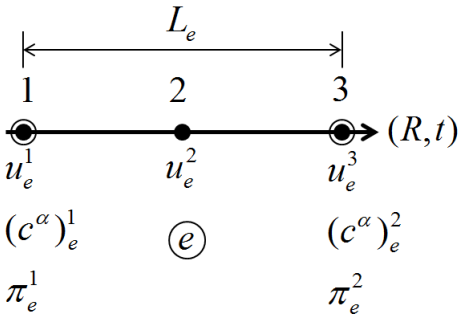

Figure 3.4: Mixed formulation.

3.3.2 Shape functions

In order to discretize the weak form to formulate the Garlerkin form, shape functions need to be defined clearly. But even under the centro-symmetric assumption, the spherical coordinates need special care. Indeed, for example the gradient in spherical coordinate is completely different from the gradient in cartesian coordinates. Extra care needs to be taken at this step.

The shape functions are defined according to the number of nodes for each phase. The solid phase shape functions are then quadratic, whereas the other phases have linear shape functions:

$$\delta \mathbf{F} = \mathbf{B}_0 \delta \mathbf{r}^e \tag{3.16}$$

$$\delta \mu^\alpha = \mathbf{N}[\delta \mu^\alpha]^e \tag{3.17}$$

$$\delta \pi = \mathbf{N}[\delta \pi]^e \tag{3.18}$$

$$\delta z = \mathbf{N}_0[\delta z]^e \tag{3.19}$$

$$\delta w = \mathbf{N}[\delta w]^e \tag{3.20}$$

where the shape functions and their derivatives are defined as:

$$\mathbf{N} = \begin{bmatrix} N_1 & N_2 \end{bmatrix} = \begin{bmatrix} \frac{1-\xi}{2} & \frac{1+\xi}{2} \end{bmatrix} \tag{3.21}$$

$$\mathbf{N}_0 = \begin{bmatrix} N_1^0 & N_2^0 & N_3^0 \end{bmatrix} = \begin{bmatrix} \frac{\xi}{2}(\xi-1) & 1-\xi^2 & \frac{\xi}{2}(\xi+1) \end{bmatrix} \tag{3.22}$$

$$\mathbf{B} = \begin{bmatrix} \frac{\partial N_1}{\partial R} & \frac{\partial N_2}{\partial R} \end{bmatrix} = \begin{bmatrix} \frac{-1}{l_e} & \frac{1}{l_e} \end{bmatrix} \tag{3.23}$$

$$\mathbf{B}_0 = \begin{bmatrix} \frac{\partial N_1^0}{\partial R} & \frac{\partial N_2^0}{\partial R} & \frac{\partial N_3^0}{\partial R} \\ \frac{2N_1^0}{R} & \frac{2N_2^0}{R} & \frac{2N_3^0}{R} \end{bmatrix} = \begin{bmatrix} \frac{2}{l_e}(\xi-\frac{1}{2}) & \frac{2}{l_e}(-2\xi) & \frac{2}{l_e}(\xi+\frac{1}{2}) \\ \frac{\xi}{R}(\xi-1) & \frac{2}{R}(1-\xi^2) & \frac{\xi}{R}(\xi+1) \end{bmatrix} \tag{3.24}$$

$$\mathbf{B}_1 = \begin{bmatrix} \frac{\partial N_1}{\partial R} & \frac{\partial N_2}{\partial R} \\ \frac{2N_1}{\partial R} & \frac{2N_2}{\partial R} \end{bmatrix} = \begin{bmatrix} \frac{-1}{l_e} & \frac{1}{l_e} \\ \frac{1-\xi}{R} & \frac{1+\xi}{R} \end{bmatrix} \tag{3.25}$$

3.3.3 Solid phase

First, we note that the unit volume of a sphere is calculated by

$$d\Omega = (RdR)(Rsin(\theta)d\theta)(d\phi) = R^2 dR(sin(\theta)d\theta)d\phi \tag{3.26}$$

Discretizing Eq. (3.13):

$$\sum_{n=1}^{n_{elt}} 4\pi \int_{\Omega_0^e} R^2 (\mathbf{B}_0[\delta z]^e)^T \mathbf{P}^v dR = \sum_{n=1}^{n_{elt}} 4\pi \int_{\Omega_0^e} R^2 (\mathbf{N}_0[\delta z]^e)^T b_0 dR + \sum_{n=1}^{n_{elt-front}} \int_{\Gamma_0^e} (\mathbf{N}_0[\delta z]^e)^T t_0 dS_0 \tag{3.27}$$

$$\sum_{n=1}^{n_{elt}}([\delta z]^e)^T 4\pi \int_{\Omega_0^e} R^2 \mathbf{B}_0^T \mathbf{P}^v dR = \sum_{n=1}^{n_{elt}}(\delta \mathbf{z}^e)^T 4\pi \int_{\Omega_0^e} R^2 \mathbf{N}_0^T b_0 dR + \sum_{n=1}^{n_{elt-front}} (\delta \mathbf{z}^e)^T \int_{\Gamma_0^e} \mathbf{N}_0^T t_0 dS_0 \tag{3.28}$$

Because δz is chosen as an arbitrary weighting function:

$$\sum_{n=1}^{n_{elt}} 4\pi \int_{\Omega_0^e} R^2 \mathbf{B}_0^T \mathbf{P}^v dR = \sum_{n=1}^{n_{elt}} 4\pi \int_{\Omega_0^e} R^2 \mathbf{N}_0^T b_0 dR + \sum_{n=1}^{n_{elt-front}} \int_{\Gamma_0^e} \mathbf{N}_0^T t_0 dS_0 \tag{3.29}$$

3.3.4 Alpha phase

Using Eq. (3.16) in Eq. (3.2.4), the latter becomes:

$$\begin{aligned}\sum_{n=1}^{n_{elt}} \Bigg(& \int_{\Omega_0^e} \frac{\partial \mathbf{N}[C^\alpha]^e}{\partial t} \mathbf{N}[\delta w]^e dV_0 + \int_{\Omega_0^e} \mathbf{N}[\dot{u}]^e (\mathbf{B}_1 [C^\alpha]_{n-1}^e)^T \mathbf{N}[\delta w]^e dV_0 \\ & + \int_{\Omega_0^e} (\mathbf{D}^\alpha k_B T (\mathbf{B}_1 [C^\alpha]^e)) \cdot \mathbf{B}_1 [\delta w]^e dV_0 + \int_{\Omega_0^e} (\mathbf{D}^\alpha \nu^\alpha C^\alpha (\mathbf{B}_1 [\pi]^e)) \cdot \mathbf{B}_1 [\delta w]^e dV_0 \Bigg) \\ & = \sum_{n=1}^{n_{elt-front}} \left(- \int_{\Gamma_0^e} i_0^\alpha \mathbf{N}[\delta w]^e dS_0 - \int_{\Gamma_0^e} i_0^\pi \mathbf{N}[\delta w]^e dS_0 \right)\end{aligned} \tag{3.30}$$

$$\begin{aligned}\sum_{n=1}^{n_{elt}} [\delta w]^{eT} \Bigg(& \int_{\Omega_0^e} \mathbf{N}^T \mathbf{N} \frac{\partial [C^\alpha]^e}{\partial t} dV_0 + \int_{\Omega_0^e} \mathbf{N}^T \mathbf{N} [\dot{u}]^e (\mathbf{B}_1 [C^\alpha]_{n-1}^e)^T dV_0 \\ & + \int_{\Omega_0^e} k_B T \mathbf{B}_1^T \mathbf{D}^\alpha \mathbf{B}_1 [C^\alpha]^e dV_0 + \int_{\Omega_0^e} \nu^\alpha C^\alpha \mathbf{B}_1^T \mathbf{D}^\alpha \mathbf{B}_1 [\pi]^e dV_0 \Bigg) \\ & = \sum_{n=1}^{n_{elt-front}} [\delta w]^e \left(- \int_{\Gamma_0^e} \mathbf{N}^T i_0^\alpha dS_0 - \int_{\Gamma_0^e} \mathbf{N}^T i_0^\pi dS_0 \right)\end{aligned} \tag{3.31}$$

Because of the arbitrary choice of δw, the equation takes the form:

$$\sum_{n=1}^{n_{elt}} \left(\int_{\Omega_0^e} \mathbf{N}^T \mathbf{N} \frac{\partial [C^\alpha]^e}{\partial t} dV_0 + \int_{\Omega_0^e} \mathbf{N}^T \mathbf{N} [\dot{u}]^e (\mathbf{B}_1 [C^\alpha]_{n-1}^e)^T dV_0 \right.$$
$$\left. + \int_{\Omega_0^e} k_B T \mathbf{B}_1^T \mathbf{D}^\alpha \mathbf{B}_1 [C^\alpha]^e dV_0 + \int_{\Omega_0^e} \nu^\alpha C^\alpha \mathbf{B}_1^T \mathbf{D}^\alpha \mathbf{B}_1 [\pi]^e dV_0 \right)$$
$$= \sum_{n=1}^{n_{elt-front}} [\delta w]^e \left(- \int_{\Gamma_0^e} \mathbf{N}^T i_0^\alpha dS_0 - \int_{\Gamma_0^e} \mathbf{N}^T i_0^\pi dS_0 \right) \quad (3.32)$$

3.3.5 Molecular incompressibility

Discretizing Eq. (3.15):

$$\sum_{n=1}^{n_{elt}} \left(\int_{\Omega_0^e} (J-1) \delta\xi dV_0 - \int_{\Omega_0^e} \sum_\alpha \nu^\alpha C^\alpha \delta\xi dV_0 \right) = 0 \quad (3.33)$$

$$\sum_{n=1}^{n_{elt}} \left(\int_{\Omega_0^e} (J-1) \mathbf{N} [\delta\xi]^e dV_0 - \int_{\Omega_0^e} \sum_\alpha \nu^\alpha \mathbf{N} [C^\alpha]^e \mathbf{N} [\delta\xi]^e dV_0 \right) = 0 \quad (3.34)$$

$$\sum_{n=1}^{n_{elt}} [\delta\xi]^{eT} \left(\int_{\Omega_0^e} (J-1) \mathbf{N}^T dV_0 - \int_{\Omega_0^e} \sum_\alpha \nu^\alpha \mathbf{N}^T \mathbf{N} [C^\alpha]^e dV_0 \right) = 0 \quad (3.35)$$

Because of the arbitrary choice of $\delta\xi$, it gives

$$\sum_{n=1}^{n_{elt}} \left(\int_{\Omega_0^e} (J-1) \mathbf{N}^T dV_0 - \int_{\Omega_0^e} \sum_\alpha \nu^\alpha \mathbf{N}^T \mathbf{N} [C^\alpha]^e dV_0 \right) = 0 \quad (3.36)$$

3.3.6 Summary of the Galerkin form

Solid

$$\sum_{n=1}^{n_{elt}} 4\pi \int_{\Omega_0^e} R^2 \mathbf{B}_0^T \mathbf{P}^v dR = \sum_{n=1}^{n_{elt}} 4\pi \int_{\Omega_0^e} R^2 \mathbf{N}_0^T b_0 dR + \sum_{n=1}^{n_{elt-front}} \int_{\Gamma_0^e} \mathbf{N}_0^T t_0 dS_0 \tag{3.37}$$

Alpha phase

$$\begin{aligned}\sum_{n=1}^{n_{elt}} \Bigg(& \int_{\Omega_0^e} \mathbf{N}^T \mathbf{N} \frac{\partial [C^\alpha]^e}{\partial t} dV_0 + \int_{\Omega_0^e} \mathbf{N}^T \mathbf{N} [\dot{u}]^e (\mathbf{B}_1 [C^\alpha]^e_{n-1})^T dV_0 \\ & + \int_{\Omega_0^e} k_B T \mathbf{B}_1^T \mathbf{D}^\alpha \mathbf{B}_1 [C^\alpha]^e dV_0 + \int_{\Omega_0^e} \nu^\alpha C^\alpha \mathbf{B}_1^T \mathbf{D}^\alpha \mathbf{B}_1 [\pi]^e dV_0 \Bigg) \\ & = \sum_{n=1}^{n_{elt-front}} [\delta w]^e \left(- \int_{\Gamma_0^e} \mathbf{N}^T i_0^\alpha dS_0 - \int_{\Gamma_0^e} \mathbf{N}^T i_0^\pi dS_0 \right)\end{aligned} \tag{3.38}$$

Molecular incompressibility

$$\sum_{n=1}^{n_{elt}} \left(\int_{\Omega_0^e} (J-1) \mathbf{N}^T dV_0 - \int_{\Omega_0^e} \sum_\alpha \nu^\alpha \mathbf{N}^T \mathbf{N} [C^\alpha]^e dV_0 \right) = 0 \tag{3.39}$$

It is usually more convenient to define the Galerkin form in previous equations through the phases' internal and external forces, namely:

Solid

$$\mathbf{F}_{int} - \mathbf{F}_{ext,s} = 0 \tag{3.40}$$

where

$$\mathbf{F}_{int} = \mathcal{A}\mathbf{F}^e_{int} \tag{3.41}$$

$$\mathbf{F}_{ext,s} = \mathcal{A}\mathbf{F}^e_{ext,s} \tag{3.42}$$

$$\mathbf{F}^e_{int} = 4\pi \int_{\Omega^e_0} R^2 \mathbf{B}_0^T \mathbf{P}^v dR \tag{3.43}$$

$$\mathbf{F}^e_{ext,s} = 4\pi \int_{\Omega^e_0} R^2 \mathbf{N}_0^T b_0 dR + \int_{\Gamma^e_0} \mathbf{N}_0^T t_0 dS_0 \tag{3.44}$$

Alpha phase

$$\mathbf{C}_\alpha \dot{\mathbf{y}} + \mathbf{K}_\alpha \mathbf{y} - \mathbf{F}_{ext,\alpha} = 0 \tag{3.45}$$

where

$$\mathbf{y} = \begin{bmatrix} \mathbf{u} \\ [C^\alpha] \\ [\pi] \end{bmatrix} \tag{3.46}$$

$$\mathbf{C}_\alpha = \mathcal{A}C^e_\alpha \tag{3.47}$$

$$\mathbf{K}_\alpha = \mathcal{A}K^e_\alpha \tag{3.48}$$

$$\mathbf{F}_{ext,\alpha} = \mathcal{A}F^e_{ext,\alpha} \tag{3.49}$$

$$\mathbf{K}^e_\alpha = \begin{bmatrix} 0 & \int_{\Omega^e_0} k_B T \mathbf{B}_1^T \mathbf{D}^\alpha \mathbf{B}_1 dV_0 & \int_{\Omega^e_0} \nu^\alpha C^\alpha \mathbf{B}_1^T \mathbf{D}^\alpha \mathbf{B}_1 dV_0 \end{bmatrix} \tag{3.50}$$

$$\mathbf{C}^e_\alpha = \begin{bmatrix} \int_{\Omega^e_0} \mathbf{N}^T \mathbf{N} (\mathbf{B}_1 [C^\alpha]^e_{n-1})^T dV_0 & \int_{\Omega^e_0} \mathbf{N}^T \mathbf{N} dV_0 & 0 \end{bmatrix} \tag{3.51}$$

$$\mathbf{F}^e_{ext,\alpha} = -\int_{\Gamma^e_0} \mathbf{N}^T i_0 dS_0 \tag{3.52}$$

Molecular incompressibility

$$\mathbf{F}_{int,constr} - \mathbf{F}_{ext,constr} = 0 \tag{3.53}$$

where

$$\mathbf{F}_{int,constr} = \mathcal{A}\mathbf{F}^e_{int,constr} \tag{3.54}$$

$$\mathbf{F}_{ext,constr} = \mathcal{A}\mathbf{F}^e_{ext,constr} \tag{3.55}$$

$$\mathbf{F}^e_{int,constr} = 4\pi \int_{\Omega^e_0} R^2(J-1)\mathbf{N}^T dR - 4\pi \int_{\Omega^e_0} R^2 \sum_\alpha \nu^\alpha \mathbf{N}^T\mathbf{N}[C^\alpha]^e dV_0)dR \tag{3.56}$$

$$\mathbf{F}^e_{ext,constr} = 0 \tag{3.57}$$

3.4 Linearized form

3.4.1 Solid phase

Starting with the mecanical internal force:

$$(\mathbf{F}^{int}_e)_{meca} = 4\pi \int_{\Omega^e_0} R^2 \mathbf{B}_0^T \mathbf{P} dR \tag{3.58}$$

$$\frac{1}{4\pi}\delta(\mathbf{F}^{int}_e)_{meca} = \int_{\Omega^e_0} R^2 \mathbf{B}_0^T \delta\mathbf{P} dR \tag{3.59}$$

The first and the second Piola-Kirshoff stresses can be related using the expression below:

$$\mathbf{P} = \mathbf{F}\mathbf{S} \tag{3.60}$$

$$\delta\mathbf{P} = \delta\mathbf{F}\mathbf{S} + \mathbf{F}\delta\mathbf{S} \tag{3.61}$$

The expression of $\delta\mathbf{P}$ is reinjected in the expression of $\delta(\mathbf{F}^{int}_e)_{meca}$:

$$\frac{1}{4\pi}\delta(\mathbf{F}_e^{int})_{meca} = \int_{\Omega_0^e}\left(R^2\mathbf{B}_0^T\left(\delta\mathbf{F}\mathbf{S}\right)^v\right)dR + \int_{\Omega_0^e}\left(R^2\mathbf{B}_0^T\left(\mathbf{F}\delta\mathbf{S}\right)^v\right)dR \tag{3.62}$$

$$\delta(\mathbf{F}_e^{int})_{meca} = \delta(\mathbf{F}_e^{int})_{meca}^{geo} + \delta(\mathbf{F}_e^{int})_{meca}^{mat} \tag{3.63}$$

$$\text{where } \frac{1}{4\pi}\delta(\mathbf{F}_e^{int})_{meca}^{mat} = \int_{\Omega_0^e}\left(R^2\mathbf{B}_0^T\left(\mathbf{F}\frac{\partial\mathbf{S}}{\partial\mathbf{d}}\right)^v\right)dR \tag{3.64}$$

$$\text{and } \frac{1}{4\pi}\delta(\mathbf{F}_e^{int})_{meca}^{geo} = \int_{\Omega_0^e}\left(R^2\mathbf{B}_0^T\left(\frac{\partial\mathbf{F}}{\partial\mathbf{d}}\mathbf{S}\right)^v\right)dR \tag{3.65}$$

3.4.1.1 Material stiffness

$$\mathbf{F}\delta\mathbf{S} = \begin{bmatrix} \delta S_{rr}F_{rr} & 0 & 0 \\ & \delta S_{\theta\theta}F_{\theta\theta} & 0 \\ (sym) & & \delta S_{\theta\theta}F_{\theta\theta} \end{bmatrix} = \begin{bmatrix} \delta S_{rr}F_{rr} \\ \delta S_{\theta\theta}F_{\theta\theta} \end{bmatrix} = \begin{bmatrix} F_{rr} & 0 \\ 0 & F_{\theta\theta} \end{bmatrix}\begin{bmatrix} \delta S_{rr} \\ \delta S_{\theta\theta} \end{bmatrix} \tag{3.66}$$

$$= \begin{bmatrix} F_{rr} & 0 \\ 0 & F_{\theta\theta} \end{bmatrix}\delta\mathbf{S}^v \tag{3.67}$$

$$\text{where } \mathbf{S}^v = \begin{pmatrix} S_{rr} \\ S_{\theta\theta} \end{pmatrix} \tag{3.68}$$

So we can express :

$$\frac{1}{4\pi}\delta(\mathbf{F}_e^{int})_{meca}^{mat} = \int_{\Omega_0^e}\left(R^2\mathbf{B}_0^T\begin{bmatrix} F_{rr} & 0 \\ 0 & F_{\theta\theta} \end{bmatrix}\delta\mathbf{S}^v\right)dR \tag{3.69}$$

where

$$\delta\mathbf{S} = \delta\left(\frac{\partial\Delta\hat{G}}{\partial\mathbf{E}}\right) \tag{3.70}$$

$$= \delta\left(\frac{\partial\Delta G^{el}}{\partial\mathbf{E}}\right) + \delta\left(\frac{\partial\Delta G^{mix}}{\partial\mathbf{E}}\right) - \delta\left(\frac{\partial\pi(J - \sum_\alpha \nu^\alpha C^\alpha)}{\partial\mathbf{E}}\right) \tag{3.71}$$

$$= \delta\left(\frac{\partial\Delta G^{el}}{\partial\mathbf{E}}\right) - \delta\pi\left(\frac{\partial J}{\partial\mathbf{E}}\right) - \pi\delta\left(\frac{\partial J}{\partial\mathbf{E}}\right) \tag{3.72}$$

$$\tag{3.73}$$

Moreover, one can show that

$$\frac{\partial J}{\partial\mathbf{E}} = J\mathbf{F}^{-1}\mathbf{F}^{-T} \tag{3.74}$$

which means that the Piola Kirchhoff osmotic pressure $\mathbf{\Pi}$ can be expressed as a function of the Cauchy osmotic pressure π through the expression:

$$\mathbf{\Pi} = \frac{\partial J}{\partial\mathbf{E}}\pi \qquad \text{or} \qquad \delta\mathbf{\Pi} = \delta(J\mathbf{F}^{-1}\pi\mathbf{F}^{-T}) \tag{3.75}$$

where the variation of $\mathbf{\Pi}$ can be expressed: it is assumed that $\mathbf{F}^{-1}$ remains constant, so the above expression becomes

$$\delta\mathbf{\Pi} = \mathbf{F}^{-1}\pi\mathbf{F}^{-T}\delta J + J\mathbf{F}^{-1}\mathbf{F}^{-T}\delta\pi \tag{3.76}$$

$$= J\mathbf{F}^{-1}\mathbf{F}^{-T}\delta\pi \tag{3.77}$$

Thus we get

$$\delta\mathbf{S}^v = \mathbf{C}\delta\mathbf{E}^v - \delta\mathbf{\Pi}^v \qquad \text{or} \qquad \delta\mathbf{S}^v = \mathbf{C}\delta\mathbf{E}^v - J(\mathbf{F}^{-1}\mathbf{F}^{-T})^v\delta\pi \tag{3.78}$$

where

$$\delta\mathbf{E}^v = \delta \begin{bmatrix} E_{rr} \\ 2E_{\theta\theta} \end{bmatrix} \qquad \text{and} \qquad \mathbf{C} = \frac{\partial^2 \Delta G^{el}}{\delta \mathbf{E}^2} \tag{3.79}$$

Yet, the expression can be fully linearized only if we express the variation of the Green-Lagrange strain tensor as a function of the unknowns. The relation between the Green-Lagrange strain tensor and the deformation gradient tensor is used as a starting point:

$$\mathbf{E} = \frac{1}{2}(\mathbf{F}^T\mathbf{F} - \mathbf{I}) \tag{3.80}$$

$$\delta\mathbf{E} = \frac{1}{2}(\delta\mathbf{F}\mathbf{F}^T + \mathbf{F}\delta\mathbf{F}^T) = \delta\mathbf{F}\mathbf{F} \tag{3.81}$$

$$\delta\mathbf{E}^v = \delta \begin{bmatrix} E_{rr} \\ 2E_{\theta\theta} \end{bmatrix} = \begin{bmatrix} \delta F_{rr} F_{rr} \\ 2\delta F_{\theta\theta} F_{\theta\theta} \end{bmatrix} \tag{3.82}$$

$$\delta\mathbf{E}^v = \begin{bmatrix} F_{rr} & 0 \\ 0 & F_{\theta\theta} \end{bmatrix} \begin{bmatrix} \delta F_{rr} F_{rr} \\ 2\delta F_{\theta\theta} F_{\theta\theta} \end{bmatrix} = \begin{bmatrix} F_{rr} & 0 \\ 0 & F_{\theta\theta} \end{bmatrix} \delta\mathbf{F}^v \tag{3.83}$$

In spherical coordinates, for a centro-symmetric assumption, the variation of gradient deformation can be derived:

$$\mathbf{F} = \begin{bmatrix} \frac{\partial r}{\partial R} & 0 & 0 \\ & \frac{r}{R} & 0 \\ (sym) & & \frac{r}{R} \end{bmatrix} \tag{3.84}$$

$$\mathbf{F}^v = \begin{pmatrix} \frac{\partial r}{\partial R} \\ 2\frac{r}{R} \end{pmatrix} = \begin{bmatrix} \frac{\partial N_1}{\partial r} & \frac{\partial N_2}{\partial r} \\ \frac{2N_1}{R} & \frac{2N_2}{R} \end{bmatrix} \mathbf{r}^e \tag{3.85}$$

$$\delta\mathbf{F}^v = \mathbf{B}_0 \delta\mathbf{r}^e \tag{3.86}$$

Finally, we get :

$$\frac{1}{4\pi}\delta(\mathbf{F}_e^{int})_{meca}^{mat} = \mathbf{K}_{meca,e}^{mat}\delta\mathbf{r}^e + \mathbf{K}_{meca,e}^{\pi}\delta[\pi]^e \tag{3.87}$$

$$\text{where } \mathbf{K}_{meca,e}^{mat} = 4\pi\int_{\Omega_0^e}\left(R^2\mathbf{B}_0^T\begin{bmatrix}F_{rr} & 0\\ 0 & F_{\theta\theta}\end{bmatrix}\mathbf{C}\begin{bmatrix}F_{rr} & 0\\ 0 & F_{\theta\theta}\end{bmatrix}\mathbf{B}_0\right)dR \tag{3.88}$$

$$\mathbf{K}_{meca,e}^{\pi} = -4\pi\int_{\Omega_0^e}\left(R^2J\mathbf{B}_0^T(\mathbf{F}^{-1})^v\mathbf{N}\right)dR \tag{3.89}$$

3.4.1.2 Geometric stiffness

$$\mathbf{S}\delta\mathbf{F} = \begin{bmatrix}S_{rr}\delta F_{rr}\\ 2S_{\theta\theta}\delta F_{\theta\theta}\end{bmatrix} = \begin{bmatrix}S_{rr} & 0\\ 0 & S_{\theta\theta}\end{bmatrix}\delta\begin{bmatrix}F_{rr}\\ 2F_{\theta\theta}\end{bmatrix} = \begin{bmatrix}S_{rr} & 0\\ 0 & S_{\theta\theta}\end{bmatrix}\delta\mathbf{F}^v \tag{3.90}$$

$$= \begin{bmatrix}S_{rr} & 0\\ 0 & S_{\theta\theta}\end{bmatrix}\mathbf{B}_0\delta\mathbf{r}^e \tag{3.91}$$

Thus, the geometric stiffness is

$$\frac{1}{4\pi}\delta(\mathbf{F}_e^{int})_{meca}^{geo} = \mathbf{K}_{meca,e}^{geo}\delta\mathbf{r}^e \tag{3.92}$$

$$\text{where } \mathbf{K}_{meca,e}^{geo} = \int_{\Omega_0^e}\left(R^2\mathbf{B}_0^T\begin{bmatrix}S_{rr} & 0\\ 0 & S_{\theta\theta}\end{bmatrix}\mathbf{B}_0\right)dR \tag{3.93}$$

3.4.1.3 Total stiffness of the solid

Using the expressions above of the geometric and material stiffnesses, the general stiffness is expressed as:

$$\frac{1}{4\pi}\delta(\mathbf{F}_e^{int})_{meca}^{geo} = \mathbf{K}_{meca,e}^{meca}\delta\mathbf{r}^e + \mathbf{K}_{meca,e}^{\pi}\delta[\pi]^e \tag{3.94}$$

$$\text{where } \mathbf{K}_{meca,e}^{meca} = \mathbf{K}_{meca,e}^{mat} + \mathbf{K}_{meca,e}^{geo} \tag{3.95}$$

3.4.1.4 Linearized Galerkin form for the solid phase

$$\mathbf{K}_s \delta\mathbf{y} = -\mathbf{R}_s \tag{3.96}$$

where

$$\mathbf{y} = \begin{bmatrix} \mathbf{u} \\ [C^\alpha] \\ [\pi] \end{bmatrix} \tag{3.97}$$

$$\mathbf{K}_s = \begin{bmatrix} \mathbf{K}^{meca}_{meca} & 0 & \mathbf{K}^{\pi}_{meca} \end{bmatrix} \tag{3.98}$$

$$\mathbf{R}_s = \mathbf{F}_{int} - \mathbf{F}_{ext} \tag{3.99}$$

$$\mathbf{K}^{meca}_{meca} = \mathcal{A}\mathbf{K}^{meca}_{meca,e} = \mathcal{A}\left(\mathbf{K}^{mat}_{meca,e} + \mathbf{K}^{geo}_{meca,e}\right) \tag{3.100}$$

$$\mathbf{K}^{\pi}_{meca} = \mathcal{A}\mathbf{K}^{\pi}_{meca,e} \tag{3.101}$$

$$\mathbf{F}_{int} = \mathcal{A}\mathbf{F}^{e}_{int} \tag{3.102}$$

$$\mathbf{F}_{ext,s} = \mathcal{A}\mathbf{F}^{e}_{ext,s} \tag{3.103}$$

$$\mathbf{K}^{geo}_{meca,e} = 4\pi \int_{\Omega^e_0} \left(R^2 \mathbf{B}_0^T \mathbf{S} \mathbf{B}_0\right) dR \tag{3.104}$$

$$\mathbf{K}^{mat}_{meca,e} = 4\pi \int_{\Omega^e_0} \left(R^2 \mathbf{B}_0^T \mathbf{F}\mathbf{C}\mathbf{F} \mathbf{B}_0\right) dR \tag{3.105}$$

$$\mathbf{K}^{\pi}_{meca,e} = -4\pi \int_{\Omega^e_0} \left(R^2 J \mathbf{B}_0^T (\mathbf{F}^{-1})^v \mathbf{N}\right) dR \tag{3.106}$$

$$\mathbf{F}^{e}_{int} = 4\pi \int_{\Omega^e_0} R^2 \mathbf{B}_0^T \mathbf{P}^v dR \tag{3.107}$$

$$\mathbf{F}^{e}_{ext,s} = 4\pi \int_{\Omega^e_0} R^2 \mathbf{N}_0^T b_0 dR + \int_{\Gamma^e_0} \mathbf{N}_0^T t_0 dS_0 \tag{3.108}$$

3.4.2 Alpha phase

3.4.2.1 Linearizarion of the Galerkin form

$$\sum_{n=1}^{n_{elt}} \left(\int_{\Omega_0^e} \mathbf{N}^T \mathbf{N} \frac{\partial [C^\alpha]^e}{\partial t} dV_0 + \int_{\Omega_0^e} \mathbf{N}^T \mathbf{N} [\dot{u}]^e (\mathbf{B}_1 [C^\alpha]_{n-1}^e)^T dV_0 \right.$$
$$\left. + \int_{\Omega_0^e} k_B T \mathbf{B}_1^T \mathbf{D}^\alpha \mathbf{B}_1 [C^\alpha]^e dV_0 + \int_{\Omega_0^e} \nu^\alpha C^\alpha \mathbf{B}_1^T \mathbf{D}^\alpha \mathbf{B}_1 [\pi]^e dV_0 \right)$$
$$= \sum_{n=1}^{n_{elt-front}} [\delta w]^e \left(- \int_{\Gamma_0^e} \mathbf{N}^T i_0^\alpha dS_0 - \int_{\Gamma_0^e} \mathbf{N}^T i_0^\pi dS_0 \right) \quad (3.109)$$

$$\sum_{n=1}^{n_{elt}} \left(\int_{\Omega_0^e} \mathbf{N}^T \mathbf{N} \frac{\partial [C^\alpha]^e}{\partial t} dV_0 + \int_{\Omega_0^e} \mathbf{N}^T \mathbf{N} [\dot{u}]^e (\mathbf{B}_1 [C^\alpha]_{n-1}^e)^T dV_0 \right.$$
$$\left. + \int_{\Omega_0^e} k_B T \mathbf{B}_1^T \mathbf{D}^\alpha \mathbf{B}_1 \delta [C^\alpha]^e dV_0 + \int_{\Omega_0^e} \nu^\alpha C^\alpha \mathbf{B}_1^T \mathbf{D}^\alpha \mathbf{B}_1 \delta [\pi]^e dV_0 \right) = -\mathbf{R}_\alpha \quad (3.110)$$

3.4.2.2 Time integration note

The process will be explain in section 3.5, but it is important to understand this step to realize that the alpha phase linearization depends on two matrices: the stiffness $\mathbf{K}$ and the time-dependent stiffness $\mathbf{C}$. It means that we will solve for $\delta \dot{\mathbf{y}}$. And according to [12], the equation to solve then takes the form:

$$\left(\mathbf{C}_{t+\Delta t}^{i-1} + \Delta t \mathbf{K}_{t+\Delta t}^{i-1} \right) \delta \dot{y} = - \left((\mathbf{F}_{int,\alpha})_{t+\Delta t}^{i-1} + \mathbf{C}_{t+\Delta t}^{i-1} \dot{y}_{t+\Delta t}^{i-1} \right) \quad (3.111)$$

3.4.2.3 Linearized Galerkin form for the alpha phase

$$\mathbf{C}_\alpha \dot{\mathbf{y}} + \mathbf{K}_\alpha \delta\mathbf{y} = -\mathbf{R}_\alpha \tag{3.112}$$

where

$$\mathbf{y} = \begin{bmatrix} \mathbf{u} \\ [C^\alpha] \\ [\pi] \end{bmatrix} \tag{3.113}$$

$$\mathbf{C}_\alpha = \begin{bmatrix} \mathbf{C}_\alpha^{meca} & \mathbf{C}_\alpha^\alpha & 0 \end{bmatrix} \tag{3.114}$$

$$\mathbf{K}_\alpha = \begin{bmatrix} 0 & \mathbf{K}_\alpha^\alpha & \mathbf{K}_\alpha^\pi \end{bmatrix} \tag{3.115}$$

$$\mathbf{R}_\alpha = \mathbf{F}_{int,\alpha} - \mathbf{C}_\alpha \dot{\mathbf{y}} - \mathbf{F}_{ext,\alpha} \tag{3.116}$$

$$\mathbf{C}_{\alpha}^{\alpha} = \mathcal{A}\mathbf{C}_{\alpha,e}^{\alpha} \tag{3.117}$$

$$\mathbf{C}_{\alpha}^{meca} = \mathcal{A}\mathbf{C}_{\alpha,e}^{meca} \tag{3.118}$$

$$\mathbf{K}_{\alpha}^{\alpha} = \mathcal{A}\mathbf{K}_{\alpha,e}^{\alpha} \tag{3.119}$$

$$\mathbf{F}_{ext,\alpha} = \mathcal{A}\mathbf{F}_{ext,\alpha}^{e} \tag{3.120}$$

$$\mathbf{F}_{int,\alpha} = \mathcal{A}\mathbf{F}_{int,\alpha}^{e} \tag{3.121}$$

$$\mathbf{K}_{\alpha,e}^{\alpha} = 4\pi \int_{\Omega_0^e} k_B T \mathbf{B}_1^T \mathbf{D}^{\alpha} \mathbf{B}_1 dR \tag{3.122}$$

$$\mathbf{K}_{\alpha,e}^{\pi} = 4\pi \int_{\Omega_0^e} \nu^{\alpha} C^{\alpha} \mathbf{B}_1^T \mathbf{D}^{\alpha} \mathbf{B}_1 dR \tag{3.123}$$

$$\mathbf{C}_{\alpha,e}^{\alpha} = 4\pi \int_{\Omega_0^e} \mathbf{N}^T \mathbf{N} dR \tag{3.124}$$

$$\mathbf{C}_{\alpha,e}^{meca} = 4\pi \int_{\Omega_0^e} \mathbf{N}^T \mathbf{N} (\mathbf{B}_1 [C^{\alpha}]_{n-1}^{e})^T dR \tag{3.125}$$

$$\mathbf{F}_{ext,\alpha}^{e} = -\int_{\Gamma_0^e} \mathbf{N}^T i_0^{\alpha} dS_0 - \int_{\Gamma_0^e} \mathbf{N}^T i_0^{\pi} dS_0 \tag{3.126}$$

$$\mathbf{F}_{int,\alpha}^{e} = \left(4\pi \int_{\Omega_0^e} k_B T \mathbf{B}_1^T \mathbf{D}^{\alpha} \mathbf{B}_1 dR \right) C^{\alpha} + \left(4\pi \int_{\Omega_0^e} \nu^{\alpha} C^{\alpha} \mathbf{B}_1^T \mathbf{D}^{\alpha} \mathbf{B}_1 \right) \pi \tag{3.127}$$

3.4.3 Molecular incompressibility

$$\sum_{n=1}^{n_{elt}} \left(\int_{\Omega_0^e} \delta J \mathbf{N}^T dV_0 - \int_{\Omega_0^e} \sum_{\alpha} \nu^{\alpha} \mathbf{N}^T \mathbf{N} \delta [C^{\alpha}]^e dV_0 \right) = -\mathbf{R}_{constr} \tag{3.128}$$

$$\delta J = \frac{\partial J}{\partial \mathbf{F}} : \delta \mathbf{F} = J (\mathbf{F}^{-T})^v \cdot \mathbf{B}_0 \delta \mathbf{r}^e = J [(\mathbf{F}^{-T})^v]^T \mathbf{B}_0 \delta \mathbf{r}^e \tag{3.129}$$

$$\sum_{n=1}^{n_{elt}} \left(\int_{\Omega_0^e} J \mathbf{N}^T [(\mathbf{F}^{-T})^v]^T \mathbf{B}_0 \delta \mathbf{r}^e dV_0 - \int_{\Omega_0^e} \sum_{\alpha} \nu^{\alpha} \mathbf{N}^T \mathbf{N} \delta [C^{\alpha}]^e dV_0 \right) = -\mathbf{R}_{constr} \tag{3.130}$$

$$\mathbf{K}_{constr}\delta\mathbf{y} = -\mathbf{R}_{constr} \tag{3.131}$$

where

$$\mathbf{y} = \begin{bmatrix} \mathbf{u} \\ [C^{\alpha}] \\ [\pi] \end{bmatrix} \tag{3.132}$$

$$\mathbf{K}_{constr} = \begin{bmatrix} \mathbf{K}^{meca}_{constr} & \mathbf{K}^{\alpha}_{constr} & 0 \end{bmatrix} \tag{3.133}$$

$$\mathbf{R}_{constr} = \mathbf{F}_{int,constr} - \mathbf{F}_{ext,constr} \tag{3.134}$$

$$\mathbf{K}^{meca}_{constr} = \mathcal{A}\mathbf{K}^{meca}_{constr,e} \tag{3.135}$$

$$\mathbf{K}^{\alpha}_{constr} = \mathcal{A}\mathbf{K}^{\alpha}_{constr,e} \tag{3.136}$$

$$\mathbf{K}^{meca}_{constr,e} = 4\pi \int_{\Omega^e_0} \left(J\mathbf{N}^T [(\mathbf{F}^{-T})^v]^T \mathbf{B}_0 \right) dR \tag{3.137}$$

$$\mathbf{K}^{\alpha}_{constr,e} = -4\pi \int_{\Omega^e_0} \left(\sum_{\alpha} \nu^{\alpha} \mathbf{N}^T \mathbf{N} \right) dR \tag{3.138}$$

$$\mathbf{F}^{e}_{int,constr} = 4\pi \int_{\Omega^e_0} \left((J-1)\mathbf{N}^T \right) dR - 4\pi \int_{\Omega^e_0} \left(\sum_{\alpha} \nu^{\alpha} \mathbf{N}^T \mathbf{N} [C^{\alpha}]^e \right) dR \tag{3.139}$$

$$\mathbf{F}^{e}_{ext,constr} = 0 \tag{3.140}$$

3.4.4 Final linearized Galerkin form for the total mixture

$$\mathbf{C}\dot{\mathbf{y}} + \mathbf{K}\delta\mathbf{y} = -\mathbf{R} \tag{3.141}$$

$$\mathbf{y} = \begin{bmatrix} \mathbf{u} \\ [C^{\alpha}] \\ [\pi] \end{bmatrix} \tag{3.142}$$

$$\mathbf{C} = \begin{bmatrix} 0 & 0 & 0 \\ \mathbf{C}_{\alpha}^{meca} & \mathbf{C}_{\alpha}^{\alpha} & 0 \\ 0 & 0 & 0 \end{bmatrix} \tag{3.143}$$

$$\mathbf{K} = \begin{bmatrix} \mathbf{K}_{meca}^{meca} & 0 & \mathbf{K}_{meca}^{\pi} \\ 0 & \mathbf{K}_{\alpha}^{\alpha} & \mathbf{K}_{\alpha}^{\pi} \\ \mathbf{K}_{constr}^{meca} & \mathbf{K}_{constr}^{\alpha} & 0 \end{bmatrix} \tag{3.144}$$

$$\mathbf{R} = \mathbf{F}_{int} + \mathbf{C}\dot{\mathbf{y}} - \mathbf{F}_{ext} \tag{3.145}$$

3.5 Numerical integration

The element matrices are expressed by the integral of functions over the domain. In practice, these integrals are approximated by numerical integration. This is performed by adding the values of the integrand evaluated at the Gauss points. In this specific case, 8 Gauss points have been used, using the Gaussian quadrature, to calculate the numerical integrations.

	Point 1	Point 2	Point 3	Point 4
Value	-0.96028986	-0.79666648	-0.52553241	-0.18343464
Weight	0.10122854	0.22238103	0.31370665	0.36268378
	Point 5	Point 6	Point 7	Point 8
Value	0.18343464	0.52553241	0.79666648	0.96028986
Weight	0.36268378	0.31370665	0.22238103	0.10122854

Table 3.1: Coordinates and weights for a 8-points Gaussian quadrature.

Chapter 4

Implementation

Chapter 3 has established the discretized weak form. This chapter explains how these equations are implemented.

4.1 Skeleton of the code

The code is constructed as follows:

(1) Input

(2) Preswelling (dry state to swollen state)

(3) Create the mesh according to the preswelling

(4) Initialize vectors and matrices

(5) Apply initial conditions from preswelling

(6) Time loop

  (a) Initialize time-dependant vectors

  (b) Initial guess for Newton's method

  (c) Apply boundary conditions

  (d) Update time-dependant vectors and unknowns

  (e) Newton-Raphson loop

(i) Initialize

(ii) Update unknows vector

(iii) Elements loop

(iii.a) Compute element vectors and Gauss-points vectors

(iii.b) Get element stiffness matrices and internal force for solid phase

(iii.c) Get element stiffness matrices and internal force for fluid phase

(iii.d) Get element stiffness matrices and internal force for matrix molecules phase

(iii.e) Get element stiffness matrices and internal force for enzymes phase

(iii.f) Assembly

(iv) Complete the assembly

(v) Compute the residual vector

(vi) Prescribe matrix and residual according to BC

(vii) Solve for $\dot{y}$

(f) Update unknown vector

(7) Postprocessing

4.2 Summary of the inputs used in the code

The inputs are all the solid, fluid, enzymes and matrix molecules parameters, as well as constants such as gas constant or Avogadro constant. See Table 4.1.

4.3 Boundary conditions

In order to solve for the numerical solutions, applying the right boundary conditions (BC) is crucial. The BC are summarized in Table 4.2.

Input name	Notation	Value	Unit	Reference
Polymer density	$\rho_{polymer}$	1.07	g/mL	Estimate
Solvent density	$\rho_{solvent}$	1	g/mL	Commonly known
True mass density (m)	ρ^{mR}	1	g/mL	Assumed
True mass density (e)	ρ^{eR}	1	g/mL	Assumed
Specific volume	$\bar{\nu}$	1	mL/g	Commonly known
Polymer charact. ratio	C_n	4	-	[31]
Average bond length	l	1.47	Å	[31]
Temperature	T	310	K	Physiological temperature
Tortuosity	δ	2	-	[20]
Fluid viscosity	$\bar{\mu}_f$	0.65E-3	N.s/m2	[38]
Solvent molecules volume	ν^f	1E-28	m3	[45]
Hydrolytic degradation rate	k	0.18	/day	Found for experiments fitting
Flory-Huggins parameter	χ_{sf}	0.467	-	[10]
Gyration radius of enzymes	r_e	20	Å	[41]

Table 4.1: Inputs and parameters.

	Change in μ	Traction test	General formulation
u	Dir. isotropic swelling (R_c)	Dir. $u(R_c) = 0$, Neumann (R_g)	-
c^f	Dirichlet $\mu(R_g) = \mu^{ext}$	Dirichlet $\mu(R_g) = \mu^{ext}$	Dirichlet $\mu(R_g) = \mu^{ext}$
c^m	Dirichlet $c^m(R_c) = 0$	Dirichlet $c^m(R_c) = 0$	Dirichlet $c^m(R_c) = c^m_{BC}$
c^e	Dirichlet $c^e(R_c) = 0$	Dirichlet $c^e(R_c) = 0$	Dirichlet $c^e(R_c) =^e_{BC}$
π	-	-	-

Table 4.2: Boundary conditions.

Chapter 5

Results

5.1 Study of the gel

5.1.1 Chemical potential test

The formulation used to define the gel is being tested to ensure the code is working properly. To check that the molecular incompressibility constraint is well applied, a Dirichlet boundary condition in R_g (outter radius) is applied so that the chemical potential is bigger outside the thin-walled gel sphere (Fig. (5.1)). As a response to equilibrate the chemical potential, fluid flows into the gel. Thus, the jacobian J increases according to Eq. (2.9). The equilibrium is reached when the inner chemical potential equals the outter one. The new jacobian, constrained by the molecular incompressibility equation, reaches the value $1 + \nu^f C^f$, which can be calculated analytically. The volume of one molecule of fluid is taken as ν^f=10E-28 m^3 [45].

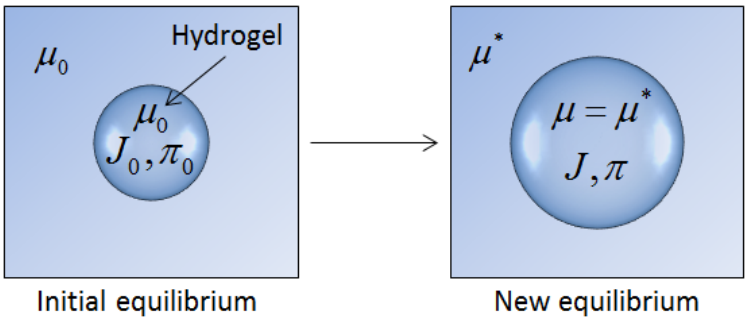

Figure 5.1: External chemical potential test

A large crosslink density suggests that the global stiffness of the gel is higher than for a small

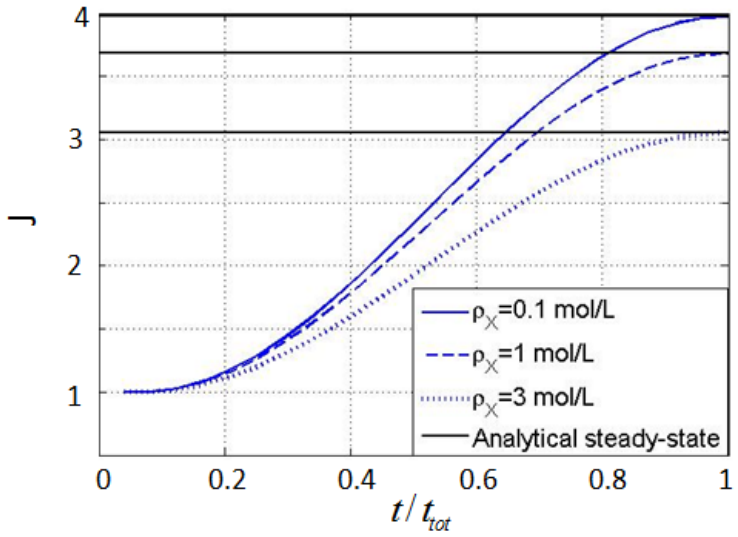

Figure 5.2: Swelling under a change of the external chemical potential for different crosslink densities

crosslink density, and so is the osmotic pressure. As a results, the swelling of a bigger crosslink density gel is smaller (Fig. (5.2)).

5.1.2 Traction test

It is common, from a mechanical scope, to investigate on the gel behavior. In order to do so, a normal traction is applied on the outter boundary of the sphere. The latter will tend to reach a new equilibrium state with an osmotic pressure π, bigger than the initial equilibrium osmotic pressure π_0.

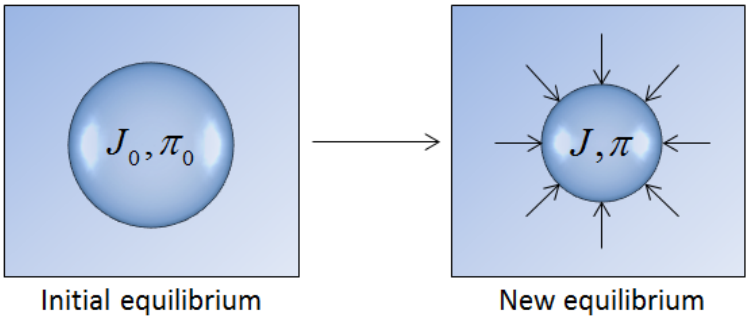

Figure 5.3: External traction test to define material stiffness

The analytical steady-state solution is solved by solving a system of three equation and three

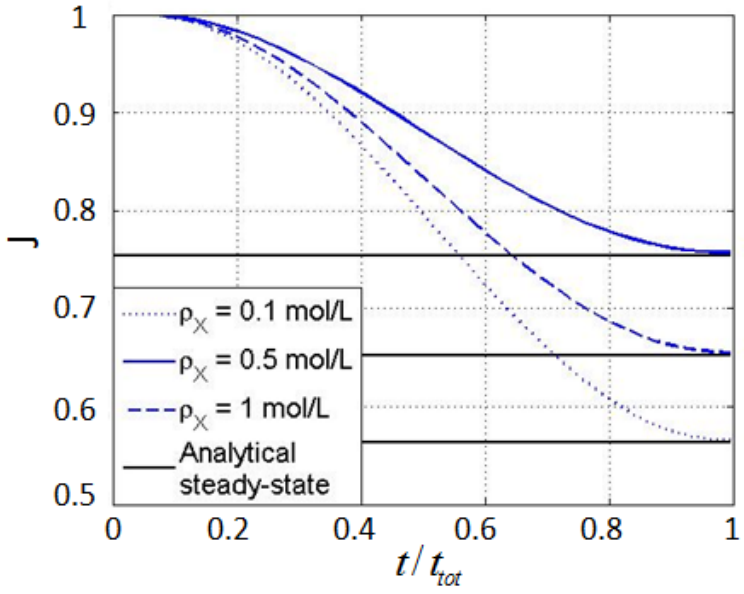

Figure 5.4: Jacobian evolution in time under an external normal traction for different crosslink densities.

unknowns J, π, C^f. Indeed, the applied traction on the sphere is known, so the first equation is Eq. (2.12). The second one is the Dirichlet boundary condition in chemical potential. And the third one is the molecular incompressibility equation, ie Eq. (2.9).

Then, Fig. (5.4) shows that for a smaller crosslink density, because the global stiffness is smaller, the compression of the sphere will be more important. Besides, for a certain repartition of the crosslink density in the scaffold, a traction test enables to determine the overall stiffness of the gel, which is important because the scaffold must not fall apart (which is likely to happen for a too fast degradation). The stiffness K is the slope of the applied pressure versus the change in jacobian plot (see Fig. (5.5)).

5.2 Hydrolytic degradation and its effect on matrix molecules diffusion

5.2.1 Degradation of the scaffold

First, when only the hydrolytic degradation occurs, the degradation of the scaffold is spatially homogeneous (Eq. (2.29)). As time evolves, the scaffold is degradaded leading to a decrease in the

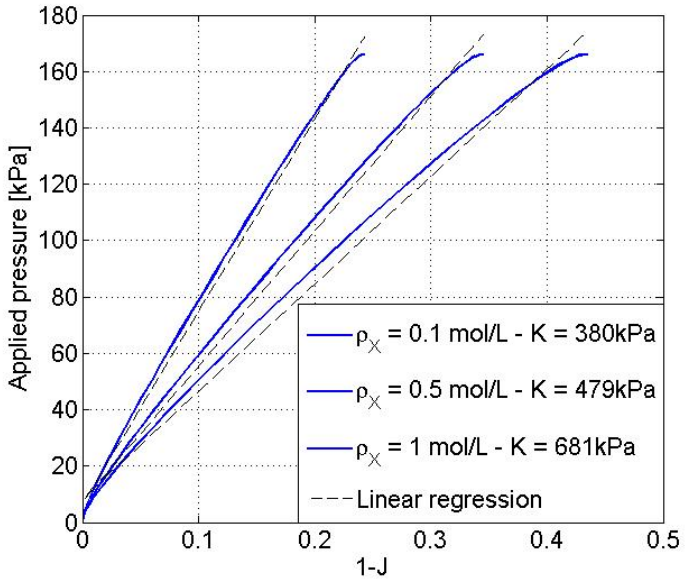

Figure 5.5: Determination of the stiffness through the traction test.

crosslink density. As a result, the osmotic pressure is decreasing, enabling fluid to flow into the swelling sphere. But also, because the crosslink density decreases, the global stiffness of the gel sphere decreases. Values of the stiffness are calculated using the traction test on the sphere for different inputs of crosslink density. In Fig. (5.6), the experimental values for the swelling evolution are matched using a hydrolytic degradation $k = 0.18/\text{day}$.

While crosslinks are degraded, the stiffness of the gel decreases, enabling fluid to flow into the gel, resulting in a swelling of the gel. Fig. (5.6) shows that the stiffness of the gel is decreasing fast, because hydrolytic degradation is a global degradation. But, if the degradation is too fast compared to the diffusion of matrix molecules, these molecules do not have the time to diffuse fast enough before the gel loses its stiffness: the gel with a low stifness eventually falls apart and is not usable as a scaffold.

In order to describe the phemomenon, dimensionless constants are defined to describe the competition between degradation and diffusion:

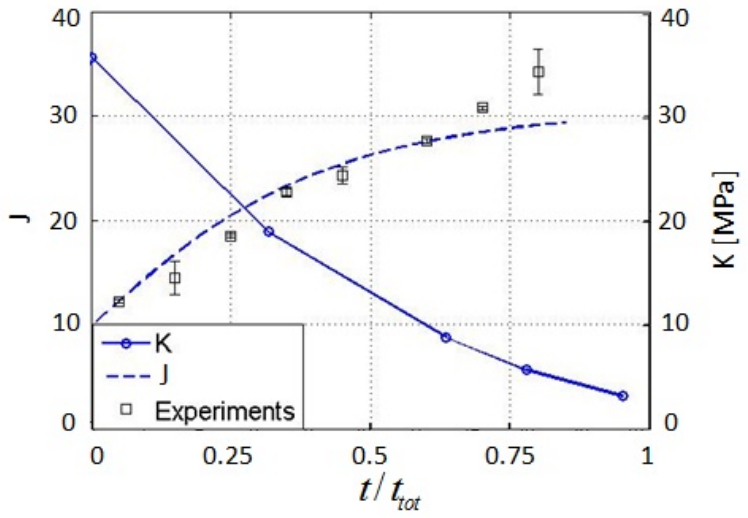

Figure 5.6: Evolution of the swelling ratio and the global stiffness of the gel under hydrolytic degradation

$$\Phi^e = \frac{r_e^2 k_2}{D^e} \quad , \quad \Phi^m = \frac{r_m^2 k_2}{D^m} \quad , \quad \Phi^h = \frac{r_m^2 k}{D^m} 1\text{E}9 \tag{5.1}$$

where r_e and r_m are respectively the radius of gyration of an enzyme molecule and of a matrix molecule. Typically, this ratio is small in a diffusion-dominated case phenomena, and takes large value when diffusion is limited. These definitions are useful to look into two different possibilities of evolution: reaction-limited or diffusion-limited. A reaction-limited case means that the degradation is happening too slow compared to the diffusion of the molecules. On the contrary, a diffusion-limited case suggests that the diffusion of the molecules is too slow, and thus, because the scaffold is degrading faster than the diffusion is occuring, the gel will lose its stiffness and fall apart before the matrix molecules are diffused enough through the gel.

5.2.2 Effect of hydrolytic degradation on molecules diffusion

The concentration of matrix molecules diffusion into the gel is directly affected by the ratio Φ^h. When this ratio takes large values (Fig. (5.7)b.), the concentration of molecules in time tends to evolve slowly, because it suggests a slow degradation of the scaffold. Whereas a small Φ^h

(Fig. (5.7)a.) suggests a fast degradation of the crosslinks and a great diffusion of the molecules in the gel.

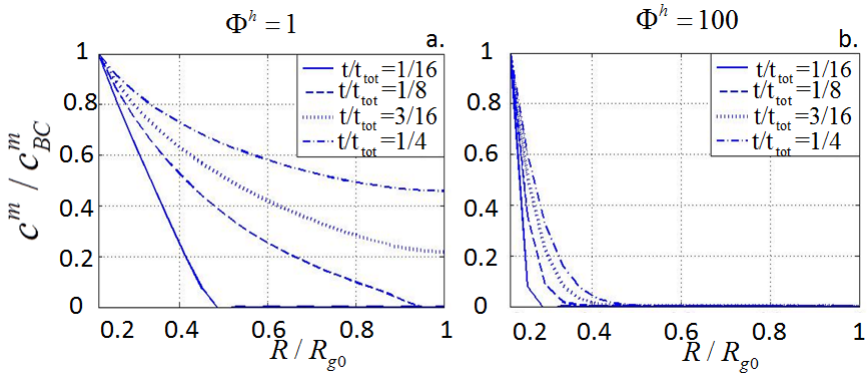

Figure 5.7: Concentration of matrix molecules for different hydrolytic degradation rates.

Because the hydrolytic degradation is a spatially homogeneous degradation, an increase of the degradation process generates a increase in the loss of global stiffness. And the faster the scaffold is degraded, the faster the matrix molecules can diffuse. But then, a great diffusion of the molecules means a fast decrease of the global stiffness. On the contrary, preserving the stiffness requires a small rate of degradation and thus a poor diffusion of the molecules in the gel (Fig. (5.8)).

A tool is created to construe the homogeneity of the molecules distribution in the gel. Note that this general definition can be used for any variable. The average value, $\bar{c}^m$, of the concentration c^m is defined as:

$$\bar{c}^m(t) = \int_{R_c}^{R_g} c^m(R,t)dR \tag{5.2}$$

5.3 Gel behavior under enzymatic degradation

When hydrolytic degradation is used, it enables the matrix molecules to diffuse because of the increasing mesh size. But, when the crosslinks are degraded homogeneously, the scaffold is likely to lose its mechanical properties, especially its global stiffness. Cell-mediated degradation

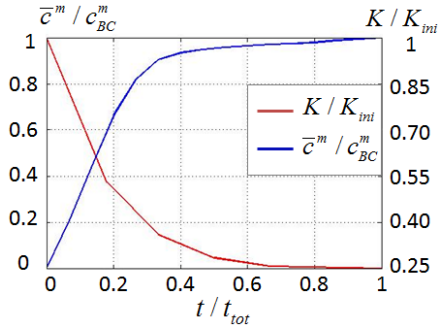

Figure 5.8: Evolution of the matrix molecules diffusion and the global stifness of the gel under hydrolytic degradation.

enables matrix molecules to diffuse through the hydrogel at the same rate the enzymatically susceptible crosslinks are being degraded. Then, the global stiffness could be preserved while matrix molecules are diffusing. On the first hand, as Φ^e increases, the concentration in enzymes gets smaller

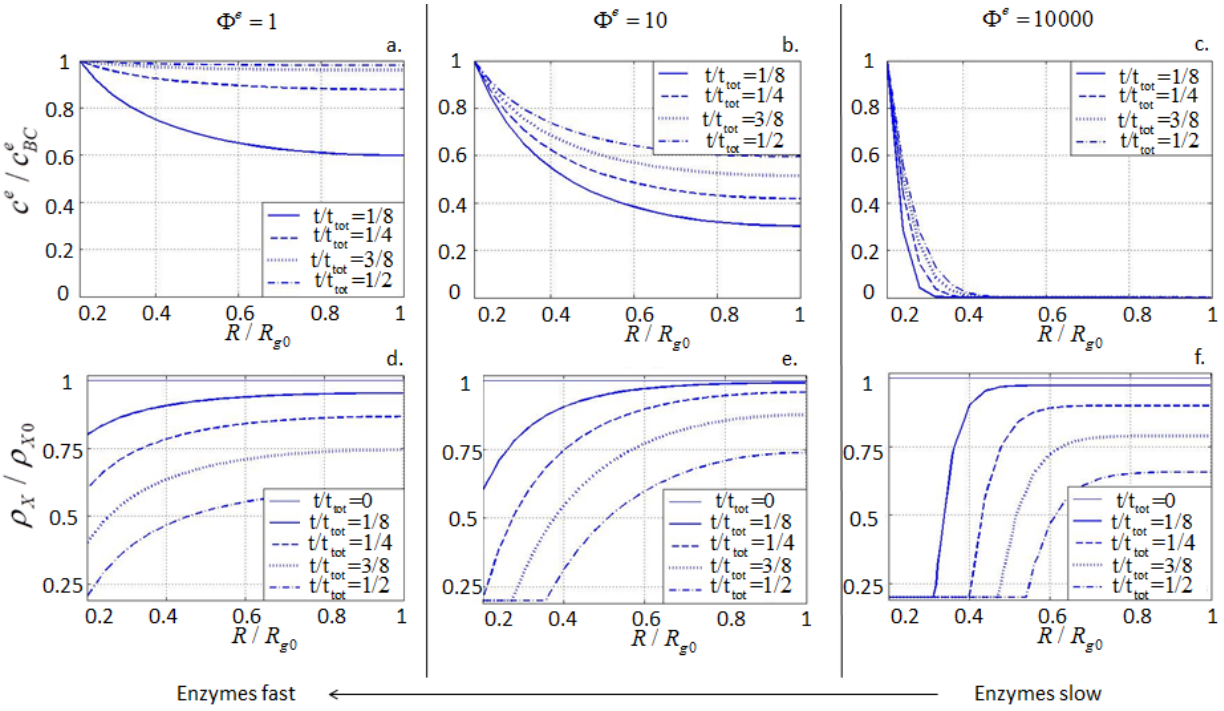

Figure 5.9: Evolution of the enzymes concentration and the crosslink density through the gel for different values of Φ^e.

(Fig. (5.9)a., b. and c.): the evolution of the enzymes falls into the diffusion-limited scheme. On the other hand, for small Φ^e, the diffusion is dominating the reaction.

Moreover, large Φ^e values denote a large enzymes degradation to diffusion ratio, such that enzymes diffuse slowly. This leads to the creation of a front (Fig. (5.9)f.) in the crosslink density spatial distribution. The scaffold is degraded as the enzymes diffuse. But, when the evolution is reaction-limited, the enzymes tend to degrade the scaffold more homogeneously (Fig. (5.9)a.).

5.4 Molecules diffusion into the gel

In order for the tissue to be a success, the unbound matrix molecules should diffuse at a reasonable rate into the gel thanks to the degradation process. In Fig. (5.10) are shown different cases of the matrix molecules concentration evolution in time while varying the two ratios Φ^e and Φ^m. Indeed, varying Φ^e gives several different possible evolutions of the enzymes, which have a huge effect on the crosslink density repartition in the gel and thus on the diffusion of the matrix molecules. But also, Φ^m is taking for different values to show the differences in behavior when the ratio of the matrix molecules diffusion rate to the enzymes diffusion rate is changing.

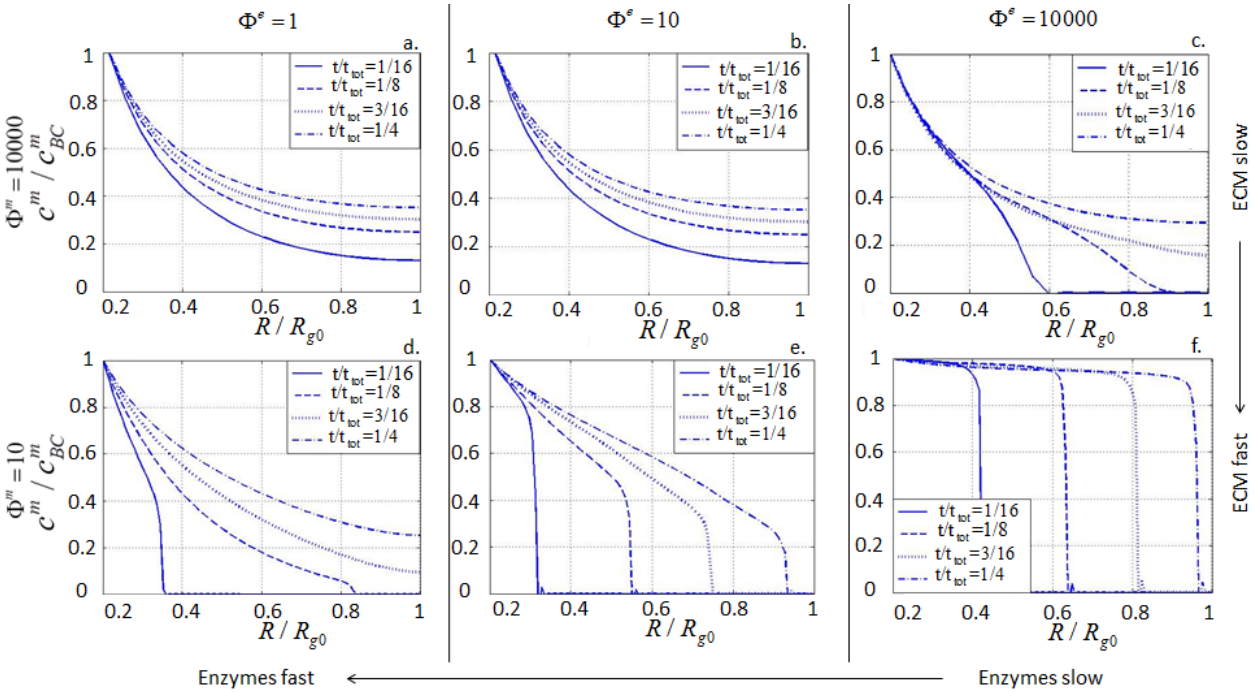

Figure 5.10: Diffusion of the matrix molecules into the gel for different values of Φ^e and Φ^m.

First, for a large value of Φ^m (Fig. (5.10)a., b., c.) the diffusion of the matrix molecules is

slow compared to the degradation rate. For small values of Φ^e, ie when the enzymes degradation to diffusion is small, the enzymatic degradation rate is much faster than the matrix molecules rate. In consequence, the matrix molecules diffusion is not affected by the mesh size of the scaffold and can diffuse freely, independently from the enzymes diffusion. Indeed, if the crosslink density has already been degraded enough (Fig. (5.10)a., b., c.), the mesh size allow matrix molecules to diffuse. But for small values of Φ^m the ratio Φ^e is directly affecting the diffusion of the matrix molecules. If the mesh size has not been degraded enough, it might not allow for the diffusion of the matrix molecules. Indeed, the bigger Φ^e gets, the more trouble matrix molecules have to diffuse. And in the case of a very large Φ^e (Fig. (5.10)f.), because the matrix molecules diffusion is faster than the enzymes diffusion, the matrix molecules have no choice than diffusing at the same rate as the enzymes. When Φ^e is large, Fig. (5.9)f. showed that a front is created in the crosslink density. Then, the mesh size after this front is too small to allow matrix molecules to diffuse, making them wait for the enzymes to degrade the scaffold.

5.5 Study of the stiffness of the gel

The failure of an engineered-tissue is often due to the loss of stiffness of the scaffold before the matrix molecules have diffused enough in the gel. It results in a loss of the integrity of the gel. However, as degradation is necessary for the molecules diffusion, the stiffness of the scaffold is meant to degrade, allowing diffusion of the molecules. These molecules will attach to the scaffold and become linked to it. This phenomena has not been put into the model. However, it is assumed that the stiffness of the matrix cannot increase until the crosslink density have been fully degraded (unpublished studies from Bryant, S. J.).

The model does not include how the molecules are getting linked to the scaffold, which is complicated. Because the matrix stiffness increases only where the scaffold is fully degraded, it is assumed that the matrix stiffness is increasing according to the coordinate of the front of crosslink density (Fig. (5.9)). If it is not completely degraded, R_{front}/R is 0 (and thus the stiffness of the matrix is 0). However when all the scaffold is entirely degraded, the coordinate of the front is

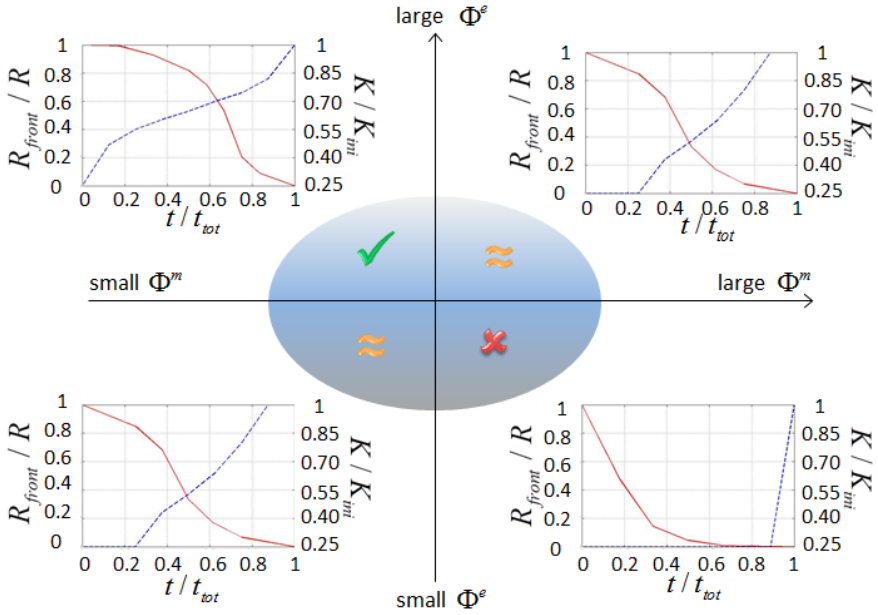

Figure 5.11: The stiffness loss versus gain of matrix stiffness in time for different degradation to diffusion ratios. Dashed line (in blue) corresponds to the newly created matrix stiffness, and plain line (in red) represents the overall stiffness of the scaffold.

maximum and thus $R_{front}/R = 1$. Fig. (5.11) shows how the overall scaffold stiffness and matrix stiffness evolve in time for different ratios Φ^e and Φ^m. It is important to remember that the goal is that the matrix stiffness becomes large enough before the overal scaffold stiffness has lost its integrity. First, when Φ^e is small and Φ^m is large (bottom right in Fig. (5.11)) are small values, the enzymatic degradation devolve into a hydrolytic degradation type. Because the degradation is spatially homogeneous, the matrix stiffness can never increase until all the scaffold has been degraded and therefore, the scaffold loses all its stiffness which results in a failure of the creation of tissue. In the case of both small or large Φ^e and Φ^m (bottom left and top right in Fig. (5.11)), the behavior shown is symmetric. The new matrix stiffness is increasing thanks to a crosslink density distribution showing a small front. But still, it can be seen that the matrix stiffness is not increasing fast enough compared to the loss of scaffold stiffness. To solve this issue, the matrix stiffness would have to increase faster, or the scaffold stiffness should decrease slower. This is what is happening in the case of a large Φ^e and a small Φ^m (top left in Fig. (5.11)). Actually, because the crosslink

density shows and evolution of a moving front in time (Fig. (5.9)) and thus the matrix molecules concentration maximum when diffused (Fig. (5.10), it allows the stiffness of the new matrix to increase faster. But also, the front evolution of crosslink density enables the scaffold stiffness to stay high longer.

Chapter 6

Concluding remarks

Along this thesis, we have built a mathematical model of the ECM growth using a thermodynamical approach. Poromechanics has been used in order to combine the different phases involoved in the process, and finite-element method has been used to build the mathematical model by coding it in MATLAB. Finally, results have been made and an analysis of the results has been done to understand how an enzymatic degradation affect the diffusion of the matrix molecules and thus the creation, or not, of the ECM itself.

Tissue growth is based in the diffusion of the matrix molecules into the gel. But on order to diffuse the scaffold has to be degraded and thus decrease its stiffness momentarily. The loss of stiffness of the scaffold so that the stiffness of the matrix coming from the matrix molecules counterbalance this loss is what determine the success or the failure of the phenomenon. If the loss is fast and too important, the scaffold lose its stiffness and is no longer a solid. If the loss of stiffness is too slow because the degradation is too slow, the molecules cannot diffuse and thus the matrix will not be created.

Hydrolytic degradation can be used to degrade the scaffold, but it has been seen through the study that it is not possible to degrade the scaffold properly for the molecules to diffuse and the matrix stiffness to increase. If the degradation is too fast, then the stiffness loss is too fast, and if the degradation is too slow, then the molecules are not diffused enough. And in both cases, the spatially honoeneous degradation does not allow for matrix growth. This is the reason why

enzymatic degradation is being considered. First, if the ratio of the diffusion of the enzymes to the diffusion of the matrix molecules is small, the matrix molecules are diffused in the gel as they were freely diffusing in an already degraded enough scaffold. This case has no improvement compared to the hydrolytic degradation and must then be avoided. But, it seems that the creation of a front is a way of dealing the issue. A large ratio of the diffusion of the enzymes to the diffusion of the matrix molecules suggests that the enzymes degrade the scaffold slower than the matrix molecules are diffused. The front allows the stiffness of the new matrix to increase and the molecules have time to create the new matrix. The creation of the new matrix happens at te same time the scaffold is degraded, replacing it. Finally, creating a front seems to answer the requirements to build the matrix. A future study could be focused on the effects of the sharpness the front should be, and what are the optimum diffusions ratios in order to build a matrix with a required stiffness. Indeed, if molecules are diffused very fast compared to the enzymes, the enzymes do not have the time to degrade the scaffold. As a result, it is possible that because too many matrix molecules have been secreted, the cell is being enclosed in a very stiff matrix, making exchange of nutrients with the exterior impossible, and thus leading to the death of the cell.

Bibliography

[1] Ateshian, G. A., Kim, J. J., Grelsamer, R. P., Mow, V. C., & Warden, W. H. Finite deformation of bovine material properties cartilage compression., International Journal of Solids and Structures, 30(97) (1997)

[2] Ateshian, G. A. On the theory of reactive mixtures for modeling biological growth., Biomechanics and modeling in mechanobiology, 6:423–45 (2007)

[3] Ateshian, G. A., Costa, K. D., Azeloglu, E. U., Morrison, B. & Hung, C. T. Continuum modeling of biological tissue growth by cell division, and alteration of intracellular osmolytes and extracellular fixed charge density., Journal of biomechanical engineering, 131:101001 (2009)

[4] Armstrong, C. G. & Mow, V. C. Variations in the intrinsic mechanical properties of humanarticular cartilage with age, degeneration, and water content., The Journal of bone andjoint surgery, American volume 64:88–94 (1982)

[5] Bell, C. L., & Peppas, N. A. Biomedical Membranes from Hydrogels and Interpolymer Complexes., Polymer, 122 (1995)

[6] Boom, R. M., van den Boomgard, Th., & Smolders, C. A. Equilibrium Thermodynamics of a Quaternary Membrane-Forming System with Two Polymers. 1. Calculations., Macromolecules, 27(8) (1994)

[7] Bryant, S. J., & Anseth, K. S. Controlling the spatial distribution of ECM components in degradable PEG hydrogels for tissue engineering cartilage., Journal of biomedical materials research., Part A, 64(1):70–9. (2003)

[8] Coussy, O. Poromechanics., John Wiley & Sons (2004)

[9] Cowie, J. M. G., & Arrighi, V. Polymers : Chemistry and Physics of Modern Materials., Press : Boca Raton, Florida. (2008)

[10] Dhote, V., Skaalure, S., Akalp, U., Roberts, J., Bryant, S. J. , Vernerey, F. J. On the role of hydrogel structure and degradation in controlling the transport of cell-secreted matrix molecules for engineered cartilage., Journal of the Mechanical Behavior of Biomedical Materials, In Press, Accepted Manuscript (2012)

[11] Dimicco, M. A., & Sah, R. L. Dependence of Cartilage Matrix Composition on Biosynthesis , Diffusion , and Reaction., Transport in Porous Media, 858:57–73 (2003)

[12] Farsad, M. & Vernerey, F. J. An XFEM-based numerical strategy to model mechanical interactions between biological cells and a deformable substrate., International Journal of Numerical Methods in Engineering, 858:57–73 (2003)

[13] Flory, P. J. Principles Of Polymer Chemistry, Cornell University Press (1953)

[14] Haider, M. A., Olander, J. E., Arnold, R. F., Marous, D. R., McLamb, A. J., Thompson, K. C., Woodruff, W. R., et al. A phenomenological mixture model for biosynthesis and linking of cartilage extracellular matrix in scaffolds seeded with chondrocytes., Biomechanics and modeling in mechanobiology, 10(6):915–24 (2011)

[15] Hardingham, T. Proteoglycans and Glycosaminoglycans. Dynamics of bone and cartilage metabolism (M. J. Seib., pp. 85-98). Burlington. (2006)

[16] Holmes, M. H., & Mow, V. C. The nonlinear characteristics of soft gels and hydrated connective tissues in ultrafiltration., Journal of biomechanics, 23(11):1145–56 (1990)

[17] Hong W., Zhao X., Suo Z. Large deformation and electrochemistry of polyelectrolyte gels, Journal of the Mechanics and Physics of Solids, 58:558–577 (2010)

[18] Hootman, J. M., & Helmick, C. G. Projections of US prevalence of arthritis and associated activity limitations., Arthritis and rheumatism, 54(1):226–9 (2006)

[19] Horkay, F, Tasaki, I., & Basser, P. J. Osmotic swelling of polyacrylate hydrogels in physiological salt solutions., Biomacromolecules, 1(1):84–90 (2000)

[20] Kestin, J., Khalifa, H. E., & Correia, R. J. Tables of the Dynamic and Kinematic Viscosity of Aqueous Nael Solutions in the Temperature Range 20-150 C and the Pressure Range 0.1-35 Mpa., J. Phys. Chem. Ref. Data,10(1):71–87 (1981)

[21] Klisch, S. M., Chen, S. S., Sah, R. L. & Hoger, A. A. Growth Mixture Theory for Cartilage With Application to Growth-Related Experiments on Cartilage Explants., Journal of Biomechanical Engineering,125:169 (2003)

[22] Klisch, S. M., Asanbaeva, A., Oungoulian, S. R., Masuda, K., Thonar, E. J-MA, Sah, R. L. A cartilage growth mixture model with collagen remodeling: validation protocols., Journal of Biomechanical Engineering,130(3):031006 (2008)

[23] Kwan, M. K., Lai, W. M., & Mow, V. C. A finite deformation theory for cartilage and other soft hydrated connective tissues–I. Equilibrium results., Journal of biomechanics, 23(2):145–55 (1990)

[24] Leddy, H. A., Awad, H. A. & Guilak, F. Molecular diffusion in tissue-engineered cartilage constructs: effects of scaffold material, time, and culture conditions., Journal of biomedical materials research. Part B, Applied biomaterials, 70:397–406 (2004)

[25] Lévesque, S. G. & Shoichet, M. S. Synthesis of enzyme-degradable, peptide-cross-linked dextran hydrogels., Bioconjugate chemistry, 18:874–85 (2007)

[26] Li C., Borja R. I., Regueiro R. A. Dynamics of porous media at finite strain, Computational Methods Appl. Mech. Engrg., 193:3837–3870 (2004)

[27] Lustig, S. R., & Peppas, N. A. Solute diffusion in swollen membranes. IX. Scaling laws for solute diffusion in gels., Journal of Applied Polymer Science, 36(4):735–747 (1988)

[28] Metters, A. T., Anseth, K. S., & Bowman, C. N. Fundamental studies of a novel , biodegradable PEG-b-PLA hydrogel., Polymer, 41(May 1999), 3993-4004 (2000)

[29] Metters, A. T., Bowman, C. N., & Anseth, K. S. A Statistical Kinetic Model for the Bulk Degradation of PLA-b-PEG-b-PLA Hydrogel Networks., Society, 7043–7049 (2000)

[30] Metters, A. T., Bowman, C. N., & Anseth, K. S. Verification of Scaling Laws for Degrading PLA- b -PEG- b -PLA Hydrogels., AIChE Journal, 47(6) (2001)

[31] Merrill, E. W., Dennison, K. A., & Sung, C. Partitioning and diffusion of solutes in hydrogels of poly(ethylene oxide)., Biomaterials, 14(15):1117–26. (1993)

[32] Nicodemus G. D., Skaalure S. C. and Bryant S. J. Gel structure has an impact on pericellular and extracellular matrix deposition, which subsequentely alters metabolic activities in chondrocyte-laden PEG hydrogels, Acta Biomateralia, 7:492–504 (2011)

[33] Nicodemus, G. D. & Bryant, S. J. Cell encapsulation in biodegradable hydrogels for tissue engineering applications., Tissue engineering. Part B, Reviews, 14:149–65 (2008)

[34] Rubinstein, M., & Colby, R. H. Polymer Physics. Oxford University Press. (2003)

[35] Schacht, E. H. Polymer chemistry and hydrogel systems., Journal of Physics: Conference Series, 3:22–28 (2004)

[36] Sengers, B. G., Van Donkelaar, C. C., Oomens, C. W. J., & Baaijens, F. P. T. The local matrix distribution and the functional development of tissue engineered cartilage, a finite element study., Annals of biomedical engineering, 32(12):1718–27 (2004)

[37] Slaughter, B. V., Khurshid, S. S., Fisher, O. Z., Khademhosseini, A., & Peppas, N. A. Hydrogels in regenerative medicine., Advanced materials (Deerfield Beach, Fla.), 21(32-33):3307–29 (2009)

[38] Thorne, R. G., Hrabetova, S., & Nicholson, C. Diffusion measurements for drug design., Nature Materials, 4:713–714 (2005)

[39] Treloar, L. R. G. The Physics of Rubber Elasticity, Oxford Classic Texts (1975)

[40] Trewenack, A. J., Please, C. P., & Landman, K. A. A continuum model for the development of tissue-engineered cartilage around a chondrocyte., Mathematical medicine and biology: a journal of the IMA, 26(3):241–62 (2009)

[41] Vernerey F. J. , Greenwald E. C. and Bryant S. J. Triphasic mixture model ofcell-mediated enzymatic degradation of hydrogels, Computer Methods in Biomechanics and Biomedical Engineering, 1:1–14 (2011)

[42] Vernerey, F. J. , Foucard, L. & Farsad, M. Bridging the scales to explore cellular adaptation and remodeling., BionanoScience, 1(3):110–115 (2011)

[43] Vernerey, F. J. and Farsad, M. A Constrained Mixture Approach to Mechano-Sensing and Force Generation in Contractile Cells., Journal of the Mechanical Behavior of Biomedical Materials, 4(8):1683-1699 (2011)

[44] Yamaoka H., Asato H., Ogasawara T., Nishizawa S., Takahashi T., Nakatsuka T., Koshima I., Nakamura K., Kawaguchi H., Chung U.-I., Takato T., Hoshi K. Cartilage tissue engineering using human auricular chondrocytes embedded in different hydrogel materials, Journal of biomedical materials research, 78(1):1–11 (2006)

[45] Zhang J., Zhao X., Suo Z. & Jiang H. A finite element method for transient analysis of concurrent large deformation and mass transport in gels, Journal of Applied Physics, 105:093522 (2009)